Coordination Chemistry Reviews 254 (2010) 1038–1053

Contents lists available at ScienceDirect

Coordination Chemistry Reviews

journal homepage: www.elsevier.com/locate/ccr

Review

Synthesis and assembly of rare earth nanostructures directed by the principle of coordination chemistry in solution-based process

Wei Feng, Ling-Dong Sun, Ya-Wen Zhang, Chun-Hua Yan*

Beijing National Laboratory for Molecular Sciences, State Key Laboratory of Rare Earth Materials Chemistry and Applications & PKU-HKU Joint Lab on Rare Earth Materials and Bioinorganic Chemistry, College of Chemistry and Molecular Engineering, Peking University, Beijing 100871, China

Contents

ARTICLE INFO

Article history:
Received 21 October 2009
Accepted 5 February 2010
Available online 13 February 2010

Keywords:
Rare earth nanomaterials
Coordination chemistry
Synthesis
Assembly

ABSTRACT

In this review, several typical nanomaterials are selected to demonstrate the coordination effect on the control of structure/microstructure/texture, surface/interface, particle size and morphology. Based on the principle of coordination chemistry, with some solution-based methods including solvothermal treatment and the thermolysis of metal complex precursors, a series of novel nanostructured rare earth compounds, such as ultra-small colloidal ceria nanoparticles, highly homogenous and stable ceria–zirconia solid solutions, and high-quality rare earth oxide and fluoride nanocrystals, etc., have been prepared by elaborately controlling the synthetic parameters and reaction kinetics. In order to reveal the mechanisms of synthesis, assembly, and properties, the phase, microstructure, texture, and surface state have been characterized systematically. The main applications of coordination chemistry principle in the synthesis and assembly of rare earth nanocrystals have been summarized, which also can be extended to direct the fabrication of other nanomaterials.

1. Introduction

Rare earth materials have been widely used in the various areas such as luminescent, magnetic, and catalytic materials, by virtue of their unique properties originating from their 4f electron configurations [1–5]. The coordination chemistry of these special metal ions plays an important role in the preparation and application of the functional materials. Since early times, the principle of coordination chemistry was used in the separation of different rare earth ions by solvent extraction. Using organic coordinated ligands with different complexation affinities for rare earth ions, the rare earths can be manufactured in high purity by the countercurrent extraction process. Rare earth coordination complexes are expected to afford some new properties, for the functional materials, compared to those simple traditional rare earth materials. For example, some complexes containing Eu or other rare earth ions can absorb excitation energies with the coordinated ligands, and the following energy transfer process will excite rare earth ions to give the anticipated luminescence emission [6]. This process can effectively increase the absorption cross-section, and hence enhance the luminescence efficiency of phosphors as well. Rare earth-based single molecular magnets also utilize coordination chemistry to endow crystals with various desired structures, which ensure the effective magnetic interactions between rare earth ions [7]. Furthermore,

* Corresponding author. Tel.: +86 10 6275 4179; fax: +86 10 6275 4179.
E-mail address: yan@pku.edu.cn (C.-H. Yan).

0010-8545/$ – see front matter © 2010 Elsevier B.V. All rights reserved.
doi:10.1016/j.ccr.2010.02.007

the application of coordination chemistry in the fabrication of rare earth solid materials has also attracted the interests of scientists. Especially for the nanomaterials, the large surface to volume ratio would result in much more coordinated ligands bound at the surface than that for the common bulk materials [8]. The properties modified by these ligands will also provide some new trends for practical applications.

In recent decades, nanoscience has attracted extensive attention because of the small size and novel properties of nanomaterials, which provide ultra small composites with high packed densities, and some new functional materials [9–14]. Usually, the novel properties of nanomaterials come from four main effects specifically the quantum confinement effect, small size effect, surface effect, and dielectric confinement effect [15–17]. In the case of quantum dots, the properties are highly related to the particle size and influenced by the quantum confinement effect. For rare earth based nanomaterials, the isolated rare earth ions determine the properties. Generally, the quantum confinement effect could not be observed because the size of the nanocrystal is much larger than its Bohr radius. Therefore, surface effect is the main factor which influences the physical and chemical properties, such as size, shape, dispersibility, luminescence, and catalytic activity of nanomaterials, because surface effect generally exists in all materials and plays a more important role when the size of the materials reduces to have larger surface area.

In most cases, the surface effect comes from the different atom structures from surface relaxing lattices or the capping ligands which coordinate to the surface atoms of nanomaterials and thus stabilize the surface. Because the lattice relaxation is a spontaneous process to minimize the free energy of the surface, it is usually difficult to control as designed. As for the capping ligands, they can be varied among diverse molecular structures, and hence it is much easier to modify the surface properties through this approach. In order to saturate the coordination number of the surface rare earth ions, capping ligands must be introduced to stabilize the surface. The interactions between capping ligands and surface atoms can be divided into two main categories. One is electrostatic attraction forces between counter ions and surface charges. Electrostatic forces show no specificity, so those counter ions adsorbed on the surface only have weak interactions to the surface atoms, which can be easily substituted. The other one is the coordination bond, which originated from the interactions between metal ions and coordinated ligands. Coordination bonds usually have high bond energies, so these tightly bound capping ligands can be treated as a part of the nanomaterials, which influence the surface properties of nanomaterials and provide some new properties originating from the ligands.

Besides the influence on the properties of nanomaterials, coordination chemistry also plays an important role during the synthesis process of these nanomaterials. The main effect of the coordinated ligands in the synthesis process is the control over the concentration of metal ions, which controls the growth kinetics of nanocrystals. The passivation of the surface will also change the surface energies and influence the prefered shape of the nanocrystals, which has an indirect influence on the properties of the nanomaterials.

Considering rare earth-based materials, especially for nanosized materials, coordination chemistry also plays a significant role during the synthesis and assembly process as for the common traditional metals. In addition, because rare earth ions usually have a higher affinity for oxygen than other kinds of coordinated atoms, oxygen contained functional molecules/ions such as OH^-, inorganic oxyacid anions, fatty acid, and ethylene diamine tetraacetic acid (EDTA) are usually used as capping ligands to act on rare earth ions. The strong interactions between oxygen atoms and rare earth ions can provide more opportunities for the adjustment of surface energy and passivation of surface atoms. The strong and stable coordination bond will also allow further reactions to occur only on the ligands.

Because of the importance of rare earth materials in the materials science, some reviews have been presented to summarize the synthesis and application of rare earth functional nanomaterials [18–21]. The application of coordination chemistry principles can also be found in the description of the routine synthetic and assembly methods. Herein we will use basic coordination chemistry principles to reveal some generally employed methods for the controllable synthesis and assembly of rare earth-based functional nanomaterials, and summarize the research results obtained in our group mainly based on the rare earth nanomaterials as examples. The principles also come from the accepted viewpoints deduced from those well-studied systems such as quantum dots and other nanomaterials, and most of the protocols described here can be extended to other nanomaterials. Aspects of the luminescence and magnetic properties of rare earth materials are not included in this review.

2. Coordinated ligands as anion sources

A common route for the synthesis of elemental nanomaterials is the decomposition of appropriate precursors, or the redox reaction of the corresponding compounds. The reaction rate is easily controlled by the adjustment of the concentration of single precursor. For the synthesis of complex nanomaterials, the products come from the combination between anions and ions in the solution based coprecipitation process. The crystallization process is influenced by the concentration of both anions and cations from different sources, which make it hard to control the process. In order to control these processes, one reaction reagent is usually in excess to avoid its influence on the growth of nanocrystals. However, this method leaves a large amount of excess reagent and the compounds as byproducts, which is neither efficient nor environmentally friendly.

Single-source precursor can be applied for the synthesis of binary compound nanomaterials to avoid the problem mentioned above. The anions are released from the coordinated ligands, which exist in the precursors and coordinate with metal ions, during the decomposition of the precursors. Because the decomposition of precursor and the combination between anion and metal ion occur at the same time, the control over the growth of nanocrystals can be achieved by the adjustment of the precursor concentration.

This single-source precursor method was first applied for the synthesis of II–VI semiconductor and metal chalcogenide nanocrystals [22–24], and succeeded in preparing monodisperse nanocrystals. We have extended this method to the synthesis of rare earth compound nanocrystals. Using rare earth trifluoacetate, acetylacetonate, xanthonate as precursors, we can obtain rare earth fluoride [25,26], oxide [27,28], and sulfide [29–31], respectively. The growth process can also be controlled by the adjustment of precursor concentrations, and the detailed synthetic results will be discussed in the following sections.

3. Controllable synthesis and assembly of monodisperse nanocrystals

The size and shape control over nanocrystals during the synthesis procedure is always the key point of the nanoscience, because the properties of nanomaterials are often closely related to their size and shape [32–36]. Various factors can influence the size and shape of as-prepared nanocrystals, and some review articles have summarized the principal results obtained in recent years [37–41].

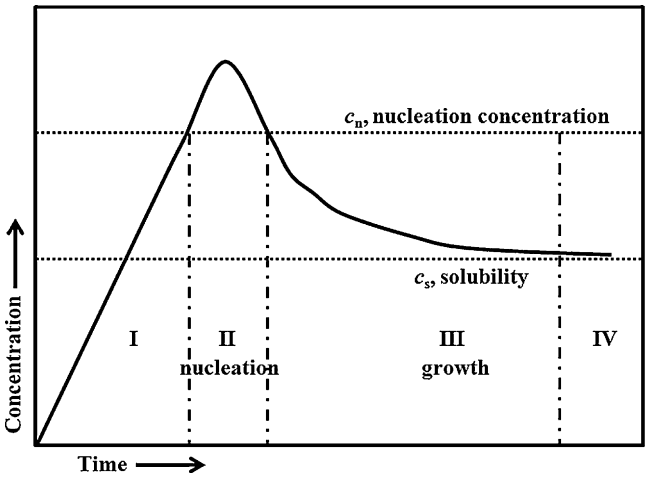

Fig. 1. LaMer curve [45], which describes the growth kinetics of crystals.

Herein, we will discuss the kinetic control and the surface passivation methods, which are the most used protocols for the control of size and shape, and introduce some recent synthetic results obtained in our group to show the application of coordination chemistry principles in these processes. In the beginning, the size control of nanocrystals via the adjustment of kinetics will be introduced.

3.1. Description of growth kinetics of nanocrystals in solution

The growth of a crystal in solution is a well-studied process [42–44]. Most results obtained in the research of crystallization processes can be extended to the growth of nanocrystals. Usually, the growth kinetics can be described by the Lamer curve [45], which divides the whole crystallization process into four main stages, named as consequent monomer accumulation, nucleation, growth, and recrystallization processes. Monomer is defined as the basic source for crystallization and usually recognized as the corresponding naked ions or molecules which directly build up the nanocrystals. As shown in Fig. 1, the concentration of monomer is realized as the key factor to determine the kinetic characteristics of the system. Two specific values, namely, nucleation concentration (c_n) and saturation concentration (c_s), are used to clarify the unsaturated, nucleation, and growth process. The first stage is the accumulation of monomer. The concentration of monomer increases in this stage by the addition of raw materials, or by the reaction from precursors. Because the concentration of monomer is below the nucleation concentration, no crystals are formed in the solution. When the concentration reaches the nucleation limit, homogeneous nucleation process will occur to form crystal nuclei in the solution (Stage II). Meanwhile, because the concentration of monomer is also higher than the solubility (saturation concentration) of the nanocrystals, all the nuclei will grow in the solution, which also consumes the monomer. The concentration of monomer will then decrease during the middle period of nucleation process, because the consumption rate for monomer will increase with the increasing nuclei number, which will finally exceed the rate for the formation of monomer. When the concentration of monomer drops back below the nucleation concentration, the nucleation process will stop, and no more nuclei will form in the solution (Stage III). After that, the solution will enter the growth stage for crystallization.

In the growth stage, all crystals formed in the nucleation process will continuously grow because the concentration of monomer is still higher than the solubility (super saturation state). According to the Thompson equation [46],

$$S_r = S_b \exp\left(\frac{2\sigma V_m}{rRT}\right)$$

where S_r and S_b are the solubility of the nanocrystal and the corresponding bulk materials, respectively, σ is the specific surface energy, r is the radius of the nanocrystals, V_m is the molar volume of the materials, R is the gas constant and T is the temperature, the smaller crystals will have a larger growth rate than larger crystals, which will cause a size-focus process to level the size of different crystals.

The next stage can be realized as a recrystallization stage (Stage IV). Along with the consumption of monomer, the concentration of monomer will decrease to a certain value just between the solubility of smaller particles and larger particles. In this stage, the smaller particles are dissolving while the larger particles are still growing, so it will further destroy the size uniformity. This process is often called Ostwald ripening.

According to the growth kinetics described above, we can deduce some useful results for the growth of nanocrystals. First, shorter nucleation process will improve the size uniformity of the products. Because all of the nuclei will grow during the nucleation and growth process, a long nucleation process will produce new small nuclei, when the early-formed nuclei have already grown to a considerable size. So the first control of crystallization for the synthesis of monodispersed nanocrystals is the burst nucleation process. Usually, this rapid nucleation is achieved by the injection of precursors into the reaction system. However a more convenient route can be used to let most of metal ions exist in the form of complexes, until the temperature reaches the thermal decomposition point to release metal ions. With the accumulation of monomer concentration above the nucleation concentration, the burst nucleation process will occur to decrease the monomer concentration, until the concentration drops back and the reaction enters the growth stage. Second, the Ostwald ripening process should be avoided, which is usually achieved by the supply of new additional monomers. This usually needs an additional operation and the time required to add raw materials is hard to control during the reaction.

As a brief summary, the synthesis of monodispersed nanocrystals will need a burst nucleation process and a following size-focus growth stage. The Ostwald ripening process should be prevented to ensure size uniformity. All of these controls are achieved by the careful adjustment of monomer concentration. The detailed analysis and experimental results can be found in the well-studied process for the synthesis of monodispersed CdSe nanocrystals [47].

3.2. Control over the monomer concentration for monodispersed nanocrystals

In most nanocrystal synthesis reactions, surfactants or some capping ligands are added to protect the nanocrystal surface. The main interactions between these additives and nanocrystals originate from the coordination effect. During the growth stage, the coordination effect between the ligands and metal ions will also affect the actual concentration of free metal ions, which will further influence the concentration of monomer and determine the growth kinetics.

The detailed control of monomer concentration by coordination can be realized as a metal buffer system as with similar situations in aqueous solutions. For a specific kind of metal ion M and ligand L, the stability constant K of complex ML, (defined as [M][L]/[ML] where [M], [L], and [ML] are the actual concentrations of the corresponding pure substances) will remain constant during the whole reaction process.

So the concentration of free metal ions is determined by the actual concentration of ML and free L molecules, which can be

further written as the following equation.

$$[M] = \frac{K[ML]}{[L]} = \frac{K(c_M - [M])}{c_L - c_M + [M]} \approx \frac{Kc_M}{c_L}$$

c_L and c_M are the total concentration of L and M added to the solution. Under common reaction conditions, the ligands are in excess relative to the metal ions. So most of metal ions are in the complex form, which means the concentration of ML is nearly the same as c_M. In this situation, the concentration of free metal ions is much lower than the total metal amount. So the concentration of M can be treated as constant determined by the total concentration of M and L. Thus, during the growth of crystals in the solution, the consumption of metal ions will be compensated by the decomposition of complex to maintain the concentration of monomers. As a result, the quasi-constant concentration of monomer will control the growth process to stay at the size-focused stage for a long time, which is necessary for the synthesis of monodisperse nanomaterials.

Based on this principle, various ligands can be used in the synthesis process to control the concentration of metal ions to modulate the growth of nanorystals. For example, rare earth phosphates and vanadates are good matrices for the luminescent materials. YVO_4:Eu and $LaPO_4$:Ce,Tb are widely used as commercial red and green phosphors, respectively [48]. The corresponding nanocrystals are also used as phosphors on the nanoscale [49–55]. Because the solubility of YVO_4:Eu and $LaPO_4$:Ce,Tb is very low in water under ambient conditions, the growth processes of these crystals are very fast in aqueous solutions, and usually lead to a non-uniform size and aggregated particles. In order to stabilize the nanoparticles and to control the growth process, we have used phosphorus containing polyacrylic acid (PAA) as ligand to coordinate with rare earth ions [18]. With the existence of PAA, YVO_4:Eu or $LaPO_4$:Ce,Tb will not precipitate by simply mixing the solutions of oxyacid anions and rare earth nitrate. During the following hydrothermal treatment, rare earth ions will react with VO_4^{3-} or PO_4^{3-} anions and crystallize in the solution. PAA molecules will also participate as the capping ligand on the surface of nanocrystals to prevent them from aggregation. The excess –COOH in PAA can be further functionalized to perform some biological usage [18,56–57].

Another route for the control over the concentration of monomer is the slow release of anions. For the synthesis of CeO_2 and CeO_2–ZrO_2 nanomaterials, urea is applied as the basic source other than NaOH [58,59]. The hydrolysis of urea slowly releases OH^- anions and controls the growth process of nanocrystals [60,61].

The principle can also be extended to the synthetic method used in organic solutions. Here we take the widely used oleic acid (OA), oleylamine (OM), and 1-octadecence (ODE) solvent system as an example. The precursors of metals are various oxysalts, which will react with oleic acid at a certain temperature to form metal oleates. In the reaction solution, the concentration of oleates is nearly the same as total metal sources, and the concentration of free metal ions is kept at a low level to control the growth of nanocrystals. During the reaction process, free metal ions will combine with the

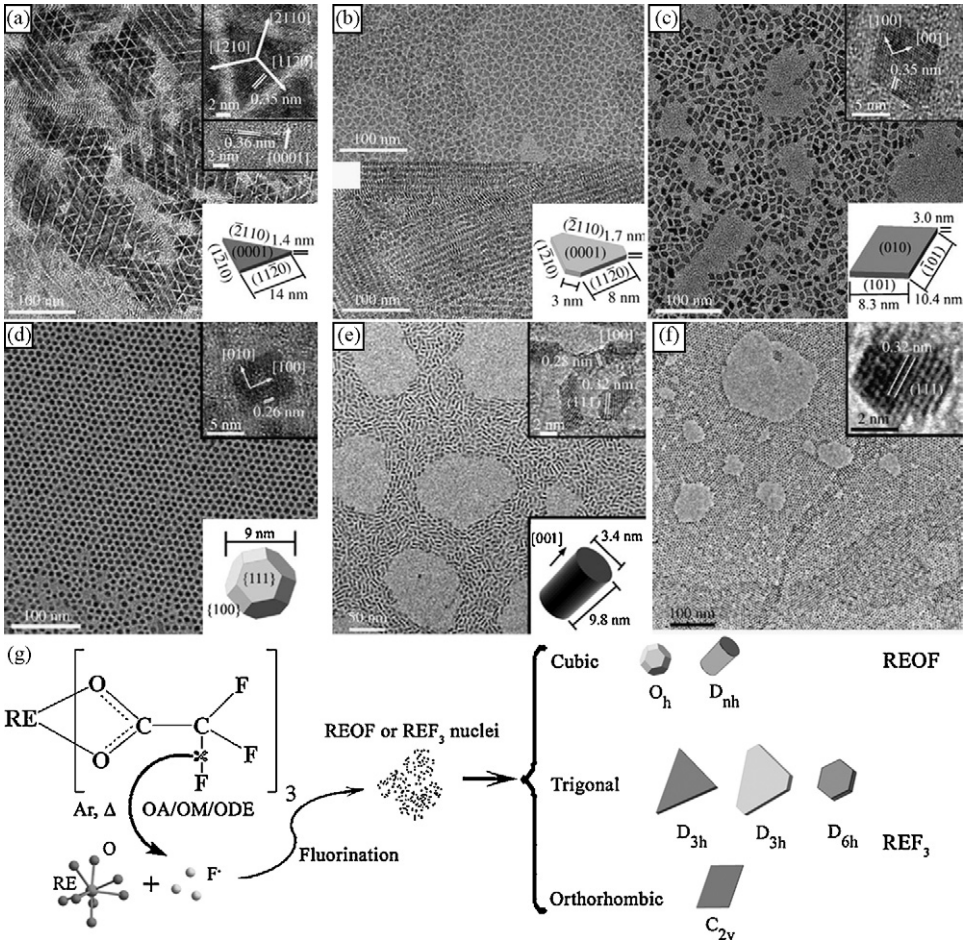

Fig. 2. The TEM images of as-prepared CeF_3 (a), NdF_3 (b), YF_3 (c) nanoplates, LuOF nanosized truncated octahedra (d), GdOF nanorods (e), and SmOF nanopolyhedra (f). The upper inset of each image is the corresponding HRTEM image, and the lower inset is the schematic diagram for each of the different shaped nanomaterials. The mechanism for the synthesis of rare earth fluoride and oxyfluoride nanocrystals from rare earth trifluoroacetate precursors through a controlled fluorination process (g).
Reprinted with permission from Ref. [70]. Copyright 2007 Wiley-VCH Verlag GmbH & Co. KGaA.

corresponding anions to form nanocrystals. Simultaneously, the oleate complex will decompose to produce new free metal ions. By the adjustment of the concentration of oleic acid and metal sources, the concentration of free metal ions can be kept between the nucleation concentration and saturation concentration, and the growth of nanocrystals will be controlled in the size-focus stage to ensure the size uniformity. This method is first used for the synthesis of FePt nanocrystals [13], and then extended to the synthesis of monodisperse nanosized metals [62,63], metal oxides [64,65], and some other complex nanomaterials [66].

Using this method, we have first synthesized LaF_3 nanoplates in OA/OM/ODE solution with rare earth trifluoroacetate as precursor [25]. After the dissolution of $La(CF_3COO)_3$ in OA solution, the coordinated ligand will be changed to OA species (in excess amount), which further forms the metal ions buffer solution. On the other hand, during the reaction, trifluoroacetate ions will supply F^- anions via a slow thermal decomposition process. The concentration of monomer will also change slowly as a result of the slow release of both F^- and rare earth ions. Therefore, the growth of nanocrystals can be well controlled in the early stage of growth process for a relatively long period, which leads to the formation of monodisperse nanocrystals.

Rare earth fluorides are useful luminescent matrices for near-infrared or upconversion emission [67–69]. With the advantage of the high transparency and damage threshold, low phonon energy, and high stability under ambient conditions, the rare earth fluorides are expected to find applications as infrared detectors, laser materials and information transports. We have extended the above

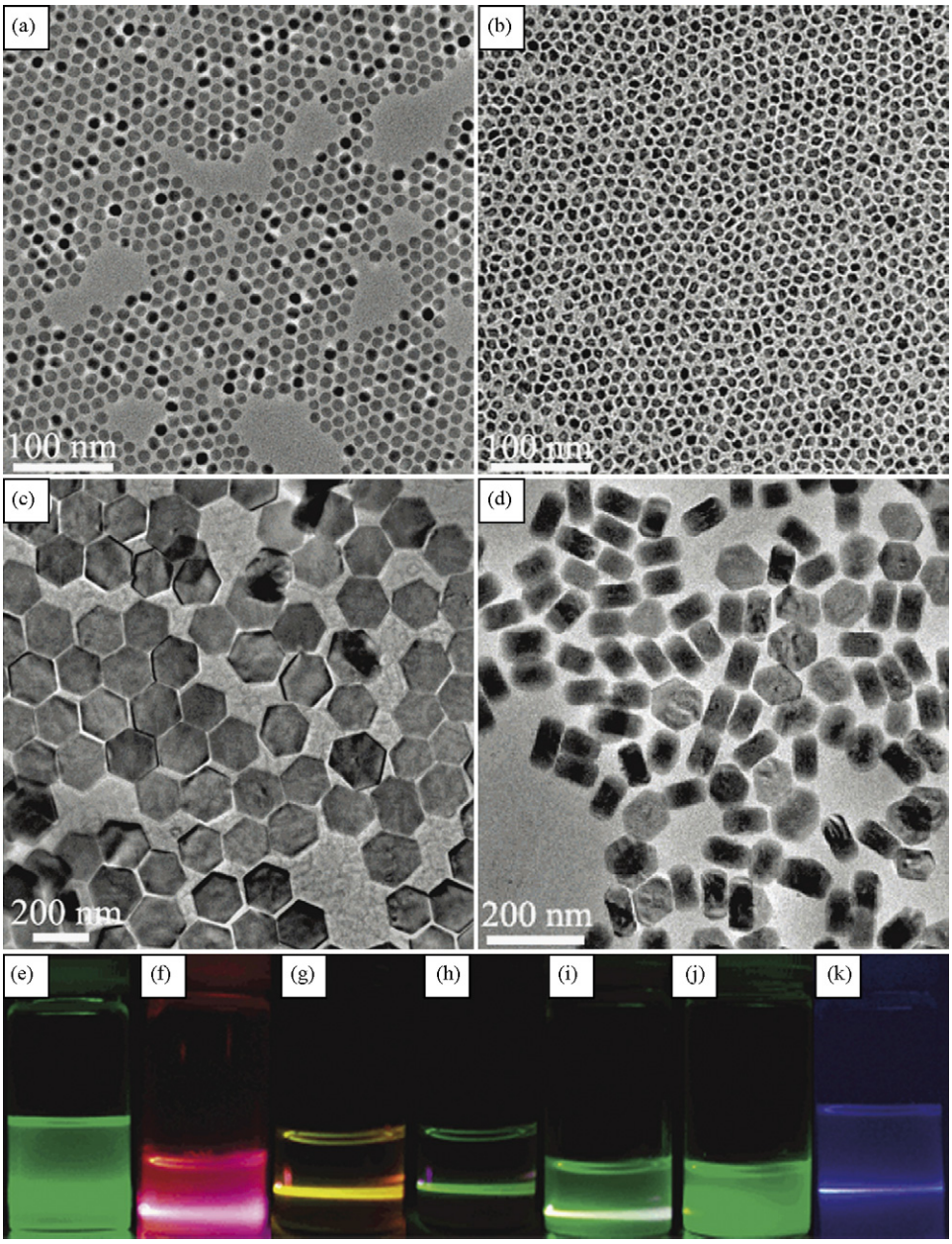

Fig. 3. TEM images of α-$NaY_{0.78}Yb_{0.2}Er_{0.02}F_4$ nanopolyhedra (a), α-$NaY_{0.695}Yb_{0.3}Tm_{0.005}F_4$ nanopolyhedra (b), β-$NaY_{0.78}Yb_{0.2}Er_{0.02}F_4$ hexagonal nanoplates (c), and β-$NaY_{0.695}Yb_{0.3}Tm_{0.005}F_4$ hexagonal nanoplates (d). Reprinted with permission from Ref. [72]. Copyright 2006 American Chemical Society. Fluorescence photographs of 185 nm β-$NaY_{0.78}Yb_{0.2}Er_{0.02}F_4$ hexagonal nanoplates (e), 5.1 nm α-$NaY_{0.78}Yb_{0.2}Er_{0.02}F_4$ nanopolyhedra (f), 8.0 nm α-$NaY_{0.78}Yb_{0.2}Er_{0.02}F_4$ nanopolyhedra (g), α-$NaY_{0.78}Yb_{0.2}Er_{0.02}F_4$@α-$NaYF_4$ nanopolyhedra (h), 20.2 nm β-$NaY_{0.78}Yb_{0.2}Er_{0.02}F_4$ nanospheres (i), β-$NaY_{0.78}Yb_{0.2}Er_{0.02}F_4$@α-$NaYF_4$ nanospheres (j), and 100 nm β-$NaY_{0.695}Yb_{0.3}Tm_{0.005}F_4$ nanoplates (k) (all excited at 980 nm; pumping power, 50 mW).
Reprinted with permission from Ref. [73]. Copyright 2007 American Chemical Society.

method to the synthesis of other rare earth fluorides as shown in Fig. 2, using the corresponding rare earth trifluoroacetates as precursors [70]. The size uniformity can be ensured by the control of the reaction time. Benefiting from the similar ionic radii and chemical activities, luminescent rare earth ions can be easily doped into those matrix materials such as LaF_3 nanocrystals by using mixed rare earth trifluoroacetate precursors. Besides the rare earth fluoride nanocrystals, oxyfluorides nanocrystals can also be obtained by a similar method (Fig. 2). Initially, all the rare earth ions are coordinated by oxygen atoms. During the reaction process, F^- anions released from trifluoroacetate anions will replace the oxygen atoms to form fluoride. We can change the amount of OM to control this fluorination process. With more OM added, OA will be further saponified to possess stronger coordination ability, in favor of the formation of rare earth oxyfluoride nanocrystals.

Another kind of widely used rare earth fluoride is the complex salt obtained through reaction with sodium fluoride. By adding sodium trifluoroacetate, the synthetic process described in the above paragraph can be used to prepare $NaYF_4$ nanocrystals and the corresponding rare earth doped nanomaterials. Usually, the cubic phase $NaYF_4$ will be obtained in the presence of OA, OM, and ODE as a kinetically controlled product. However, hexagonal phase $NaYF_4$-based materials prove to have better upconversion efficiency. We have developed a two-step method to obtain monodisperse hexagonal phase $NaYF_4$ nanocrystals [71–72]. After the first step to synthesize cubic phase nanocrystals, the products are used as starting materials in the second step, and the solvent is changed to OA and ODE. With the addition of extra sodium trifluoroacetate, hexagonal phase $NaYF_4$ nanocrystals can be prepared at a higher temperature. By doping various rare earth ions such as Yb^{3+}, Er^{3+}, or Tm^{3+}, or the control of the crystal structures of the nanomaterials, various upconversion emission bands can be observed with excitation at 980 nm (Fig. 3) [73]. The upconversion properties can be tuned by changing the phase, size, and morphology of $NaYF_4$ nanocrystals. Following a similar protocol, various reports have proved that $NaYF_4$-based monodisperse upconversion nanocrystals can be prepared [74–76], and the products have been used as biolabels and information recording media [77–79].

If we use lithium or potassium trifluoroacetates instead of sodium trifluoroacetate, $LiREF_4$ or $KREF_4$ nanocrystals can be obtained, respectively [26]. By using transition metal ions instead of rare earth ions in the presence of sodium trifluoroacetate, we can obtain $NaMF_3$ (M = Mn, Co, Ni, Mg) nanocrystals [80].

A similar method can also be used for the synthesis of rare earth oxide nanocrystals as shown in Fig. 4. In this case, we use rare earth benzoylacetonates [27], acetylacetonates, or acetates [28] as precursors. A series of rare earth oxides nanocrystals with uniform size can be obtained, and the reaction process is ascribed to the formation and following decomposition of rare earth oleates. A similar protocol has also been used for the synthesis of CeO_2 nanostructures with other ceria sources as precursors [81]. Because the process can also be realized as a double decomposition reaction

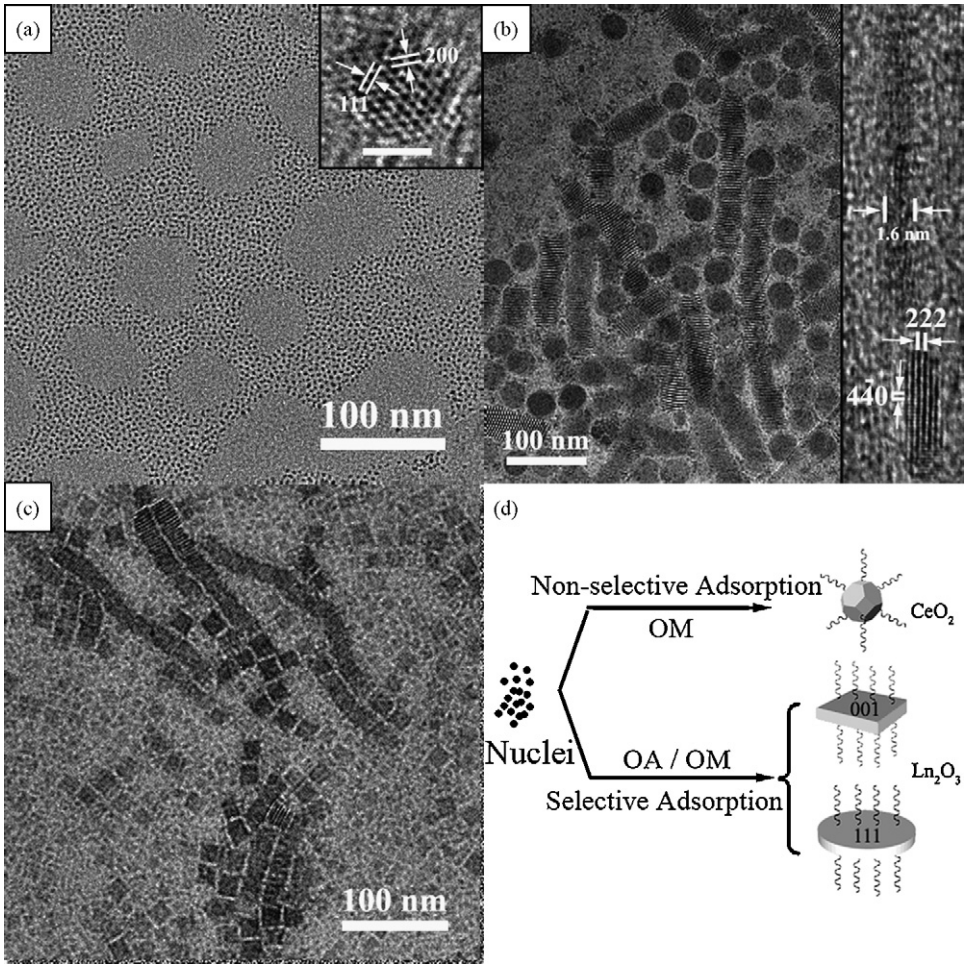

Fig. 4. TEM and HRTEM (inset) images of CeO_2 nanopolyhedra (a), Eu_2O_3 nanoplats (b), Pr_2O_3 nanodisks (c) obtained by the thermal decomposition of the corresponding rare earth benzoylacetonate precursors and the formation scheme.
Reprinted with permission from Ref. [27]. Copyright 2005 Wiley-VCH Verlag GmbH & Co. KGaA.

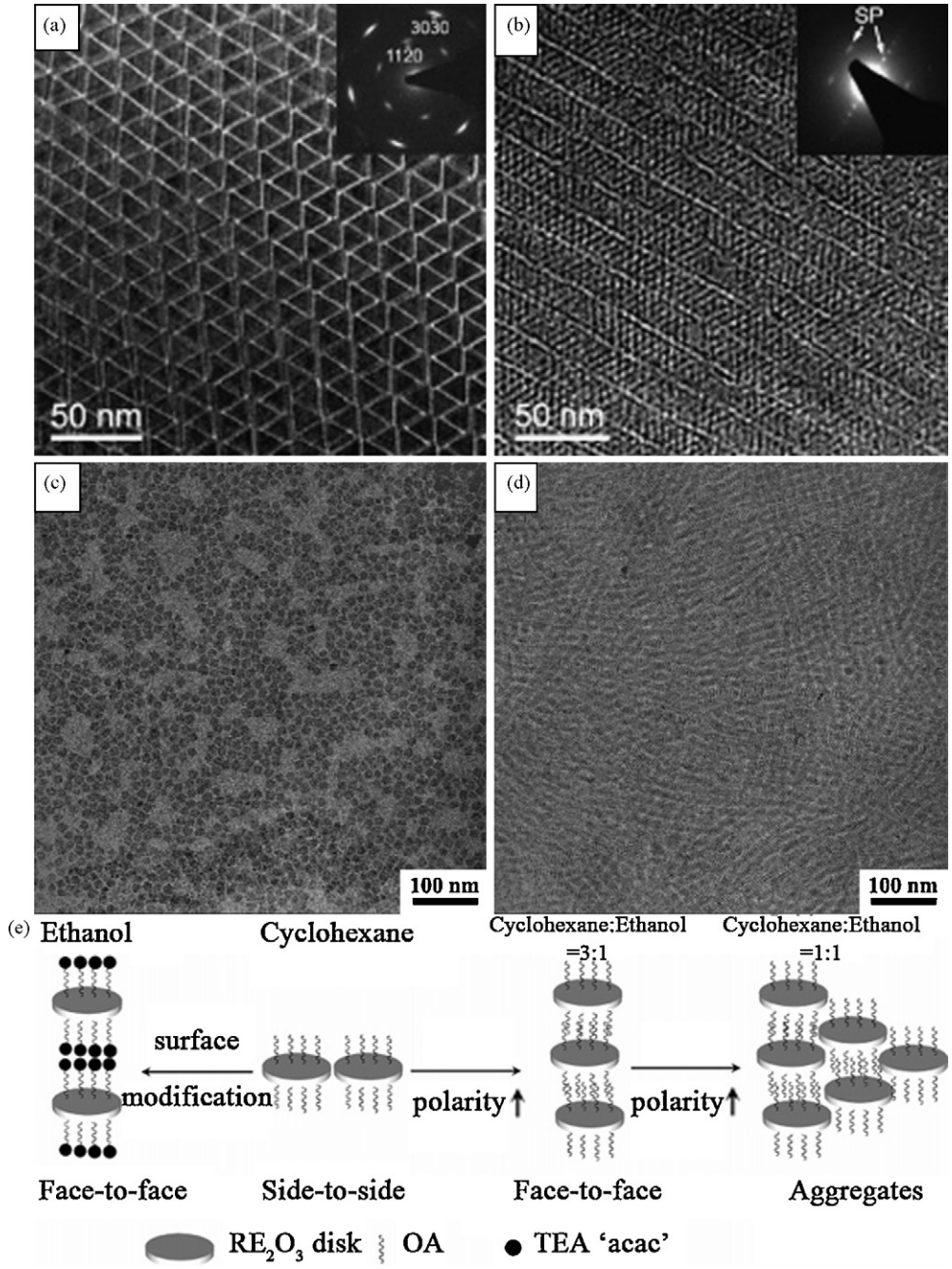

Fig. 5. TEM images of the side-to-side (a) and face-to-face (b) superlattices (SP) of LaF_3 nanoplates. Insets are the SAED patterns. Reprinted with permission from Ref. [25]. Copyright 2005 American Chemical Society. Similar TEM images of side-to-side (c) and face-to-face (d) superlattices made of Y_2O_3 nanodisks. Schematic illustration of the assembly process of nanocrystals in different solvents (e).
Reprinted with permission from Ref. [28]. Copyright 2005 Wiley-VCH Verlag GmbH & Co. KGaA.

between rare earth oleates and precipitating reagents, other rare earth oxysalts nanocrystals such as vanadates and phosphates can also be prepared with this method [82].

As mentioned above, we can synthesize monodisperse rare earth nanocrystals via a thermal decomposition method. The growth process can be well controlled by the varying of types and concentration of precursors, reaction time and temperature, and some so on. But it also has some disadvantages. The high boiling solvents are usually expensive than those common ones as water or alcohol. The byproducts originated from the decomposition of trifluoroacetate are usually toxic, which is not green for the environment. These disadvantages need to be considered in the real applications as well as their effective synthetic actions.

3.3. Surface coordinated ligands induced assembly of nanocrystals

Nanomaterials usually have the novel properties other than the traditional bulk materials, and these properties can be tuned by the size and morphology. For some real applications, large amounts of these nanomaterials with the preserved size and properties are required. Assembly is a convenient method to get aggregates com-

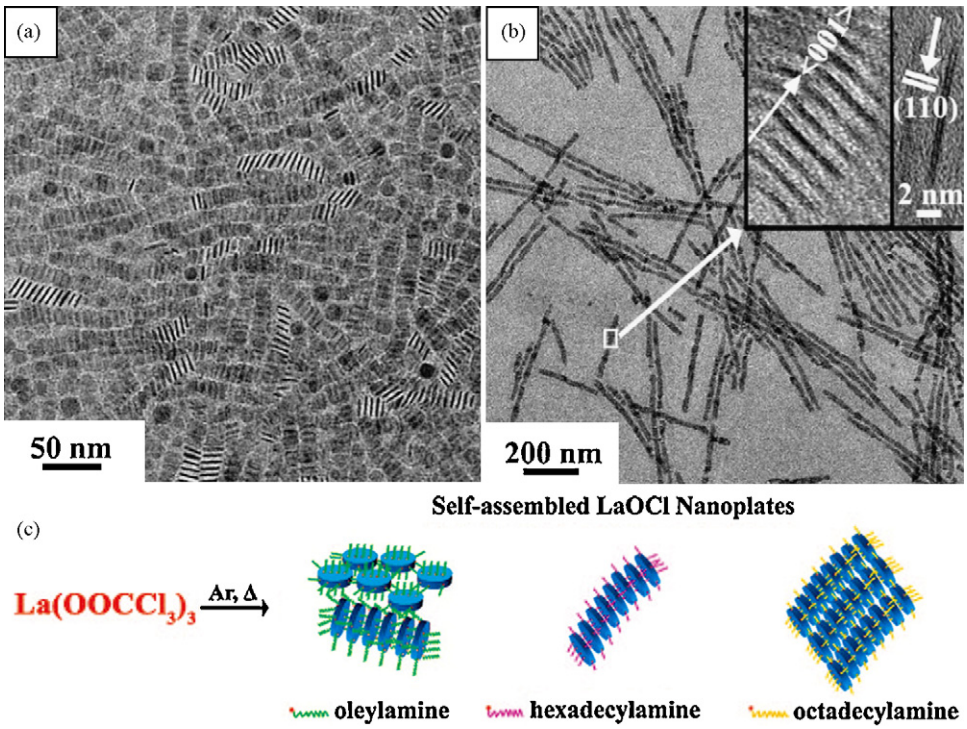

Fig. 6. TEM images of oleylamine-capped LaOCl nanoplate arrays (a), TEM and HRTEM (inset) images of nanowire-like LaOCl nanoplate arrays composed of single-linear standing nanoplates capped with hexadecylamine via the face-to-face formation (b), and the synthesis protocol of various LaOCl nanoplate arrays (c). Reprinted with permission from Ref. [103]. Copyright 2009 American Chemical Society.

posed of nanosized particles. The packed structure preserves the original size of nanomaterials with properties different from that of bulk materials [13,83–85]. Furthermore, some new or tuned properties may come from the interactions among those nanoparticles in the assembly. The assembly of nanocrystals has attracted much attention in recent years, in pursuit of finding the possible way for the real devices with new properties [86–91]. Various methods have been developed to form 2D and 3D assemblies [92–96].

Solvent evaporation induced assembly method is the well used protocol for the fabrication of large area ordered assemblies [97,98]. In this method, surface tension of the solvents proved to be the main force to determine the structure of assemblies composed of those building blocks with the size over microns [99,100]. The most common packed forms are face-centered cubic or hexagonal close packed structures. But in the case of nanocrystals, the interactions between building blocks play the most important role to determine the packed structures [101]. For those stable nanocrystals as building blocks in the solvent, capping ligands are usually coordinated to the surface of the nanocrystals to protect them from aggregation and provide the solubility in the solvent. During the assembly process, these capping ligands will provide the main forces to form the assembly. The design of these capping ligands will provide various packed structures or some new kind of functionalities [102].

Using these interactions between the ligands coordinated to the surface of nanocrystals, we succeed in tuning the assembly manner of nanostructures by using different solvents. As described in Section 3.2, LaF_3 triangle nanoplates can be synthesized in a solution composed of OA, OM, and ODE [25]. Oleic acid acts as the ligand in the solution to coordinate with metal ions to control the growth process, and also as capping ligand to protect the as-prepared nanocrystals from further growth or aggregation. In the assembly process, these oleic acid groups will pack together to form parallel structures originating from the π–π interactions and van der Waals forces between long carbon chains. In the hydrophobic solvents with low polarity, such as cyclohexane, OA molecules on the surface of nanocrystals can be extended well to the solvent based on the hydrophobic interactions. The LaF_3 nanoplates can thus be assembled into a planar close packed structure, which can be called as the side-to-side manner. Because of the regular shape, nanocrystals in the assembly have to take the same orientation, hence provide a single crystal-like electron diffraction pattern. However, the assembly architecture will be changed when we adjust the polarity of the solvent by adding ethanol. In this solvent, the dispersibility of nanocrystals will decrease, and the LaF_3 nanoplates will form a face-to-face assembled architecture. A similar phenomenon can also be observed in the assembly of rare earth oxides [28]. The side-to-side and face-to-face architectures composed of rare earth nanodisks can be obtained in cyclohexane and cyclohexane/ethanol solvent, respectively (Fig. 5).

Because the hydrophobic forces between carbon chains are the main factor to influence the assembled structures, the distance between building blocks can be tuned by changing the capping ligands on the surface. For the synthesis and assembly of rare earth oxyfluoride, we have used various amines with different chain lengths as solvent to adjust the distance in the assemblies [103]. As shown in Fig. 6, with oleylamine as capping ligand, the side-to-side and face-to-face structures coexist in the assembly. When we use hexdecylamine, LaOCl nanoplates are packed closer to each other to form a wire-like structure. Furthermore, these wire-like structures are packed further to form larger parallel structures when the ligands are changed to octadecylamine. These phenomena reveal that the assembly structure is determined by the category of capping ligands, which can be adjusted artificially.

4. Shape control of nanocrystals during the synthesis process

4.1. Template effect of coordinated ligands

Besides the control over kinetic characteristics during the crystallization process and the assembly structures, coordination effect is also widely used to control the shape of nanocrystals

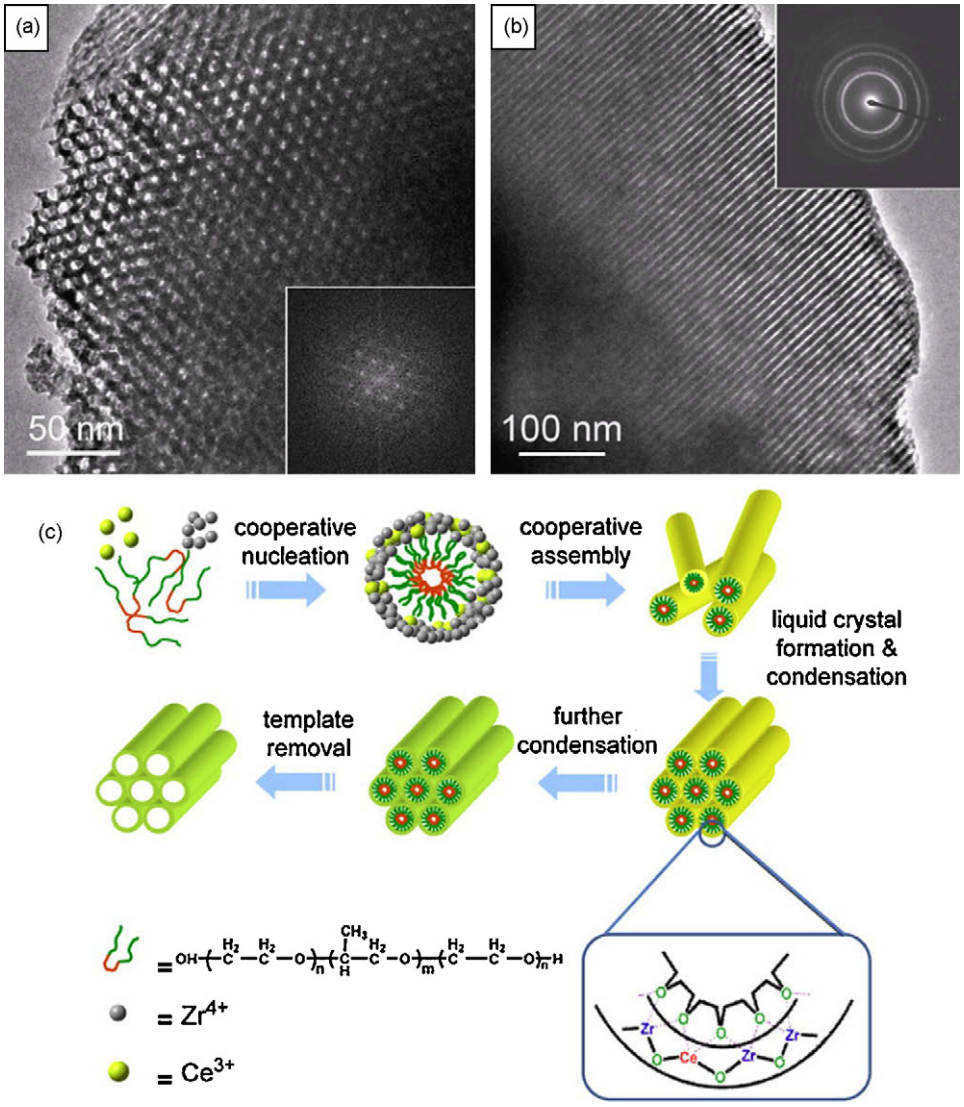

Fig. 7. TEM images of mesoporous $Ce_{0.5}Zr_{0.5}O_2$ recorded along the [0 0 1] (a) and [1 1 0] (b) orientations. The inset in (a) is the corresponding fast Fourier transform image, and the one in (b) is the corresponding selected area electron diffraction pattern. A schematic illustration (c) for the assembly process of mesoporous structures. Reprinted with permission from Ref. [119]. Copyright 2007 American Chemical Society.

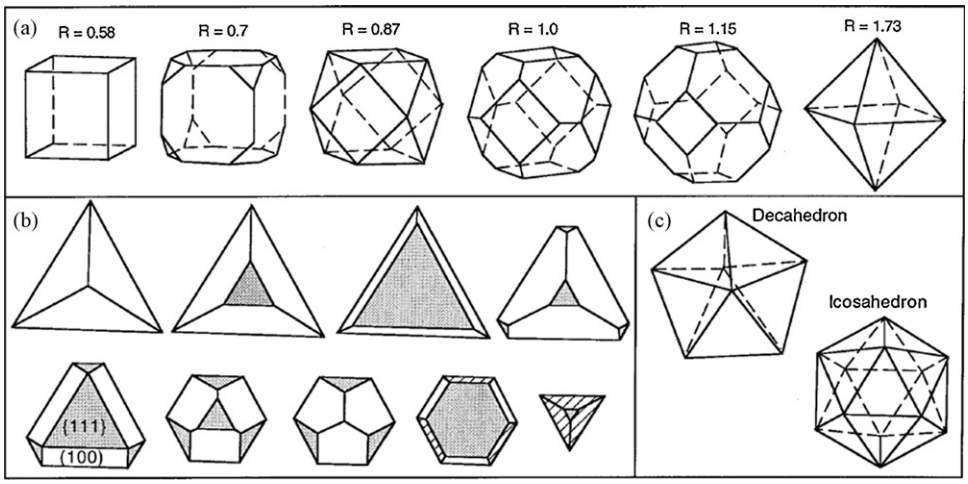

Fig. 8. Geometrical shapes of cubooctahedral nanocrystals as a function of the ratio, *R*, of the growth rate along the ⟨1 0 0⟩ to that of the ⟨1 1 1⟩ (a). Evolution in shapes of a series of (1 1 1) based nanoparticles as the ratio of {1 1 1} to {1 0 0} increases (b). Geometrical shapes of multiply twinned decahedral and icosahedral particles (c). Reprinted with permission from Ref. [123]. Copyright 2000 American Chemical Society.

[33,104–106]. Beyond the internal crystal structure determined morphology [107], the methods to modify the shape of nanocrystals during the synthesis process can be divided into two main categories. The first one is the template effect, which uses a template with designed shape and is followed by the filling in the template or growth outside the template to obtain nanocrystals with desired structures [108,109]. The template can be further divided into hard template and soft template. The most used hard template for the fabrication of nanostructures is anode aluminum oxide (AAO), which provides channels with diameters varied from tens to thousands nanometers [110]. Because the application of AAO for the shape control of nanomaterials is a well-known protocol and the shape determining mechanism has no relation to the coordination chemistry, it will not be discussed here. Another kind of important templates is micelle structures [94,111]. As well known, surfactants can form micelles in the solution. The shape of micelles is determined by the concentration of surfactants and other environmental parameters such as temperature and pressure. By employing surfactants with some functional coordination groups, metal ions will be attracted and coordinated at the surface of these micelles, and then undergo the crystallization process. In this process, micelles are used as soft template, which have tunable shape and strong interaction with metal ions.

As described in Section 3.2, we have reported that LaF_3 nanocrystals can be synthesized in the OA/OM/ODE system [25]. Because of the existence of OA and OM molecules, the shape of nanocrystals are restricted in a two dimensional area to form the triangular nanoplate, which indicates that the capping ligands form layered micelles in the solution. Similar plate-like structures are also found during the synthesis of LaOCl nanocrystals [103] (discussed in Section 3.3).

As an extension, shape control over the alkaline earth fluorides has also been achieved by the same method, because the alkaline earth metal ions have similar ionic radii and chemical properties as rare earth ions. Nanorods, nanoplates, and hollow rectangles can be obtained by tuning the composition of the solvent [112]. Because alkaline earth fluorides have cubic crystal lattices, the shape of nanoplate reveals that the growth of nanocrystals is restricted by some external factors, providing evidence for the existence of micelles as a soft template in the reaction solution.

Recently, Xia and co-workers [113] and Yang and co-workers [114] synthesized Au nanorods in the similar OA/OM/ODE system, which also confirms that the rod-like micelles in the reaction solutions act as templates for the shape evolution of Au nanorods. The coordination interaction between Au and OM is considered to be the principal effect to determine the shape of Au nanorods. Hyeon and co-workers [115] has also used this method for the fabrication of CdSe nanostructures. By the adjustment of the composition of the solution, layer-structured micelles can be formed in the solution. CdSe nanosheets can be obtained after the growth directed by these layered templates.

Similar micelles are also used as soft template to fabricate mesoporous materials with mesopores on the nanoscale. With different surfactants such as polyvinylpyrrolidone (PVP), cetyltrimethylammonium bromide (CTAB), P123, F127, etc., various mesoporous structures can be obtained by the sol-gel method. The size and shape of pores are determined by the shape of micelles [116–118].

We use a similar method to fabricate rare earth-based mesoporous structures, which attracted much interest in catalysis, due to their large surface to volume ratio and ordered pore structures. As shown in Fig. 7, P123 molecules can coordinate with Zr^{4+} and Ce^{3+} ions in the solution, and form the ordered micelle structures via a cooperative assembly process. The ordered liquid crystal phase can keep the shape and structures during the condensation process. Finally, after a calcination treatment to remove the organic species along with the oxidation of Ce^{3+} to Ce^{4+}, $Ce_{0.5}Zr_{0.5}O_2$ mesoporous

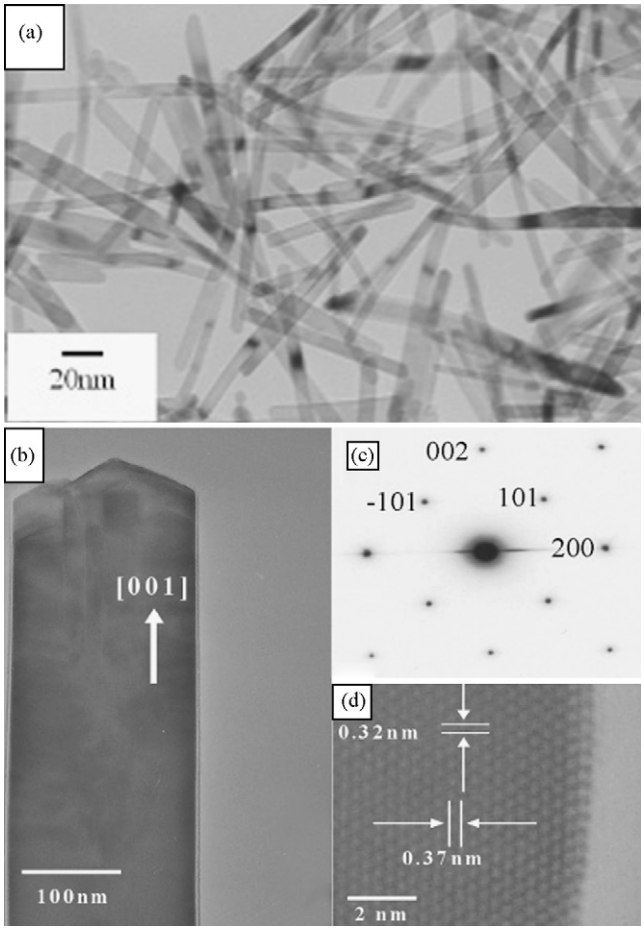

Fig. 9. SEM (a) and TEM (b) images of $CeVO_4$ nanorods prepared by the EDTA mediated hydrothermal method. The corresponding selected area electron diffraction pattern (c) and HRTEM image (d) of the sample shown in figure (b).
Reprinted with permission from Ref. [131]. Copyright 2005 American Chemical Society.

structures can be obtained [119]. Using this method, a series of zirconia-based functional mesoporous materials are synthesized, and some are used for modeling catalytic reactions [120,121]. Meanwhile, a similar method is also used for the synthesis of Al_2O_3 mesoporous nanostructures and the shape-selective catalytic properties were proven by a modeling catalytic reaction [122].

4.2. Adjustment of surface energies

The other route to control crystal shape by coordination is the adjustment of surface energies. The outer shape of crystals is determined by the types and relative area of exposure facets. For example, a crystal with a cubic lattice will favor a cubic shape if all exposed surfaces are {1 0 0} facets, and the appearance of {1 1 1} facet will lead to a truncated-octahedral shape with both {1 0 0} and {1 1 1} facets. If all exposed surfaces are {1 1 1} facets, the shape of the crystal will change to the octahedral. A similar phenomenon is shown as Fig. 8 [123], which indicates that the shape of crystals is a function as the area ratio of various facets. Usually, the area ratio of different facets is determined by the surface energies to minimize the total energy. So the adjustment of surface energy can affect the favorite shape of nanocrystals.

Because the surface of nanocrystals is usually capped by coordination species, and this passivation will effectively decrease the surface energy, the surface energy of different facets can be tuned by the facet-selective passivation, which further influences the shape of nanocrystals.

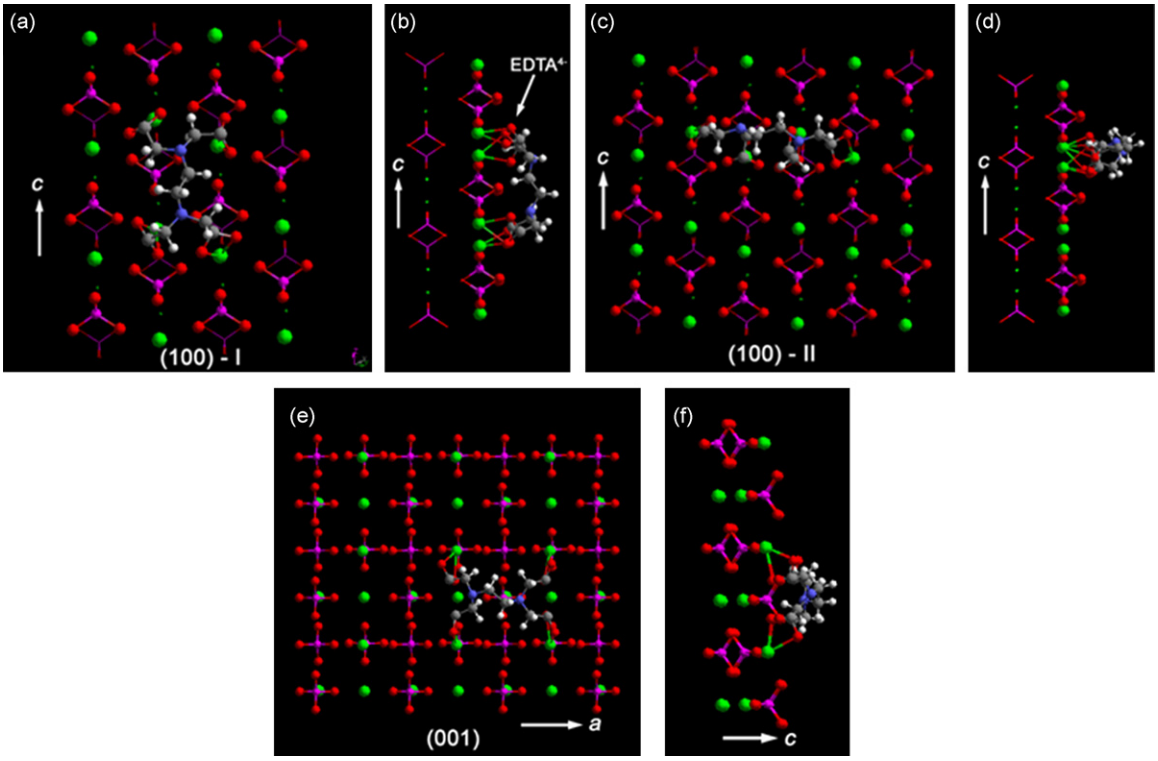

Fig. 10. Structure models for EDTA adsorbed on the different facets of *t*-$REVO_4$. Two different adsorption geometry on {1 0 0} facet (a–d) and the adsorption geometry on {0 0 1} facet (e and f). The green spheres represent rare earth atoms and red spheres represent oxygen atoms. (For interpretation of the references to color in this figure legend, the reader is referred to the web version of the article.)

For the well-studied growth process of CdSe nanocrystals [124,125], Alivisatos and co-workers [126] reported that phosphine oxide molecules will decrease the surface energies of all kinds of facets. Using an *ab initio* method, the binding of phosphine oxide on (0 0 0 1) facets proved to have the highest energies, which explains the growth of CdSe nanorods along ⟨0 0 0 1⟩ direction. A similar calculation was performed by Tang and co-workers [127] to prove that the shape of Ag nanowires produced by the polyol method is also determined by the different surface energies with the existence of PVP molecules [128–130].

In our work, the shapes of CeO_2 [81], $REVO_4$ [131], $REBO_3$ [132], and Fe_2O_3 [133] nanocrystals were also tuned successfully

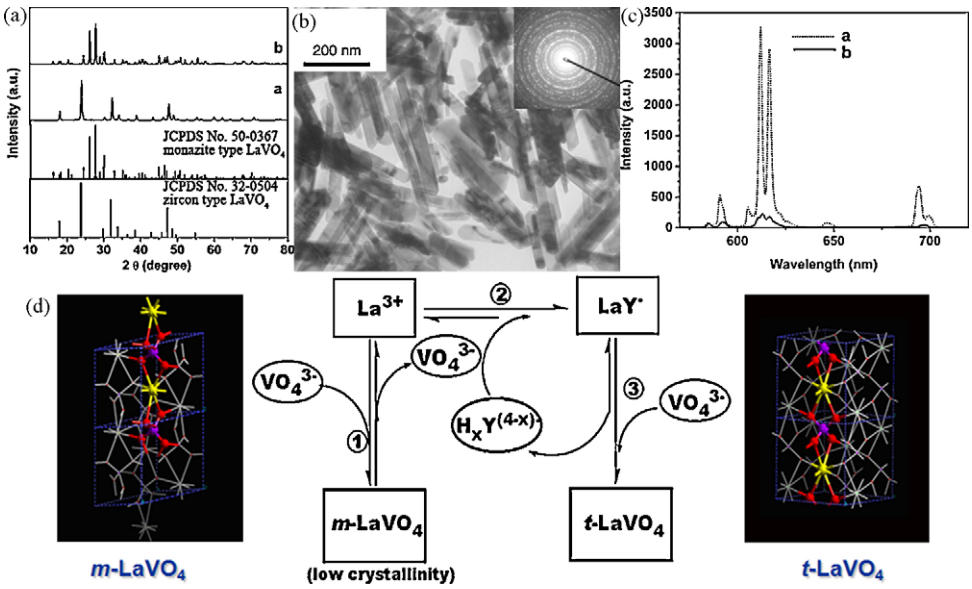

Fig. 11. XRD patterns of nanosized tetragonal $LaVO_4$:Eu (sample a), bulk monoclinic $LaVO_4$:Eu (sample b), and the corresponding standard XRD patterns of JCPDS File No. 32-0504 (tetragonal $LaVO_4$) and JCPDS File No. 50-0367 (monoclinic type $LaVO_4$) (a). TEM and selected area electron diffraction (inset) images of tetragonal $LaVO_4$:Eu nanocrystals (b). Emission spectra of nanosized tetragonal $LaVO_4$:Eu (sample a) and bulk monoclinic $LaVO_4$:Eu (sample b) with the same Eu^{3+} doping concentration (c). Schematic illustration of the formation of tetragonal $LaVO_4$:Eu from the corresponding monoclinic nanocrystals and their lattice structures (yellow and red spheres represent La and oxygen atoms, respectively) (d). (For interpretation of the references to color in this figure legend, the reader is referred to the web version of the article.)
Reprinted with permission from Ref. [146]. Copyright 2004 American Institute of Physics.

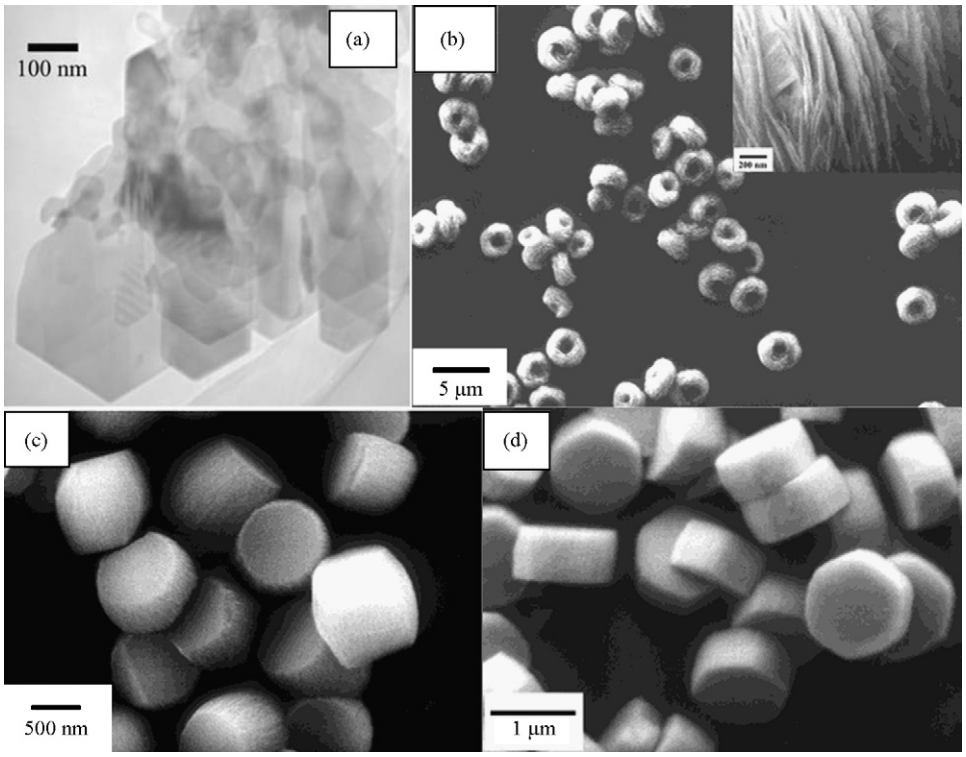

Fig. 12. TEM images of $YBO_3:Eu^{3+}$ nanocrystals with different shapes produced by the hydrothermal method. Nanosheets obtained with urea (a). Reprinted with permission from Ref. [149]. Copyright 2003 Elsevier Inc. Donut-like structures obtained with NaOH (b). Reprinted with permission from Ref. [150]. Copyright 2004 American Chemical Society. Nanodrums obtained with acetate ions (c) and nanoplates obtained with acetate ions at higher temperature (d). Reprinted with permission from Ref. [132]. Copyright 2004 American Chemical Society.

with different capping ligands to change the surface energies. CeO_2 has a cubic lattice with three simple index facets {1 0 0}, {1 1 0}, and {1 1 1}. The surface energies in vacuum have the order $\gamma\{1\,1\,1\} < \gamma\{1\,0\,0\} < \gamma\{1\,1\,0\}$ [123,134], so the most stable crystal shape is octahedral which exposes only {1 1 1} facets [135]. On the nanoscale, the high energy corner will be replaced by {1 0 0} facets to minimize total surface energy, which usually leads to a truncated octahedral shape [136]. These two types of shape are the most common ones obtained in the synthesis of CeO_2 nanocrystals. However, theoretical and experimental results have both shown that {1 0 0} facets have higher catalytic activities than {1 1 1} facets [137–141]. Yang and Gao [142] used a long chain carboxyl acid to passivate the surface of ceria nanocrystals in a high boiling point solution medium to obtain ceria nanocrystals with cubic shape. Adschiri and co-workers [143] also used a modified solvothermal method to synthesize ceria nanocrystals. Cubic shape nanocrystals can be obtained with the existence of –COOH, and the shape evolution can be examined by TEM characterization and modeling methods [144]. We have also developed a hydrothermal method to synthesize ceria nanocubes, using acetate ions as capping ligands to adjust the surface energy. These results show that the addition of –COOH groups will make the {1 0 0} facets have lower energy than {1 1 1} facets, which further induces a more stable cubic shape [145].

Another example is the hydrothermal synthesis of rare earth vanadates [131]. Rare earth vanadates usually have tetragonal lattices except $LaVO_4$. Because these rare earth vanadates all have low solubilities in the water, the corresponding nanomaterials can be synthesized directly in aqueous solution. Meanwhile, the low solubility means that the nanoparticles will crystallize immediately after the addition of raw materials, which often leads to spherical or polyhedral shaped products. In order to control the growth process and obtain products with tunable morphology, various coordinated ligands have been applied to reduce the effective concentration of metal ions and to slow down the crystallization process. We used EDTA to chelate with rare earth ions in a hydrothermal reaction to obtain rare earth vanadate nanocrystals. When the concentration of EDTA is relatively low, all ligands are used to chelate with metal ions, with no excess amount to coordinate at the surface of the products, and the products as-prepared are polyhedral. If more EDTA is added to the reaction solution, the excess EDTA will coordinate with surface metal ions of $REVO_4$ nanocrystals, further influencing the surface energies of the different facets and further determining the shape of the nanocrystals. Using this method, one dimensional $REVO_4$ nanostructures are obtained. The case of $CeVO_4$ is shown in Fig. 9 as an example. The growth direction of these nanocrystals can be determined by HRTEM characterization. ⟨0 0 1⟩ direction proved to be the preferred growth direction, which indicates that the {0 0 1} facet has the highest surface energy among those facets with low lattice indices. This difference can also be revealed by the coordination geometry on different exposure surfaces. As shown in Fig. 10, in {1 0 0} facets, rare earth ions are separated, and each EDTA anion can coordinate to four rare earth ions with four carboxy acid arms with no excess rare earth ions. But for the {0 0 1} facet, rare earth ions are much closer to each other than those in {1 0 0} facet. Hence, EDTA molecules can only coordinate with 2/3 rare earth ions due to the geometry restriction as shown in Fig. 10. Consequently, {0 0 1} facet will have higher energy than that of {1 0 0} facet. The final shape of nanostructures will be rod-like with low-energy {1 0 0} facet on the side.

The amount of EDTA can tune the shape of the nanocrystals by the adjustment of surface energies. It can also change the energy of the crystals to stabilize specific phases [146]. Tetragonal rare earth vanadates are important matrices for luminescent materials, because four V–O–RE bonds around each rare earth ions have bond angles near 153°, which is the ideal value for efficient energy transfer from VO_4^{3-} to the rare earth luminescent centers. $LaVO_4$

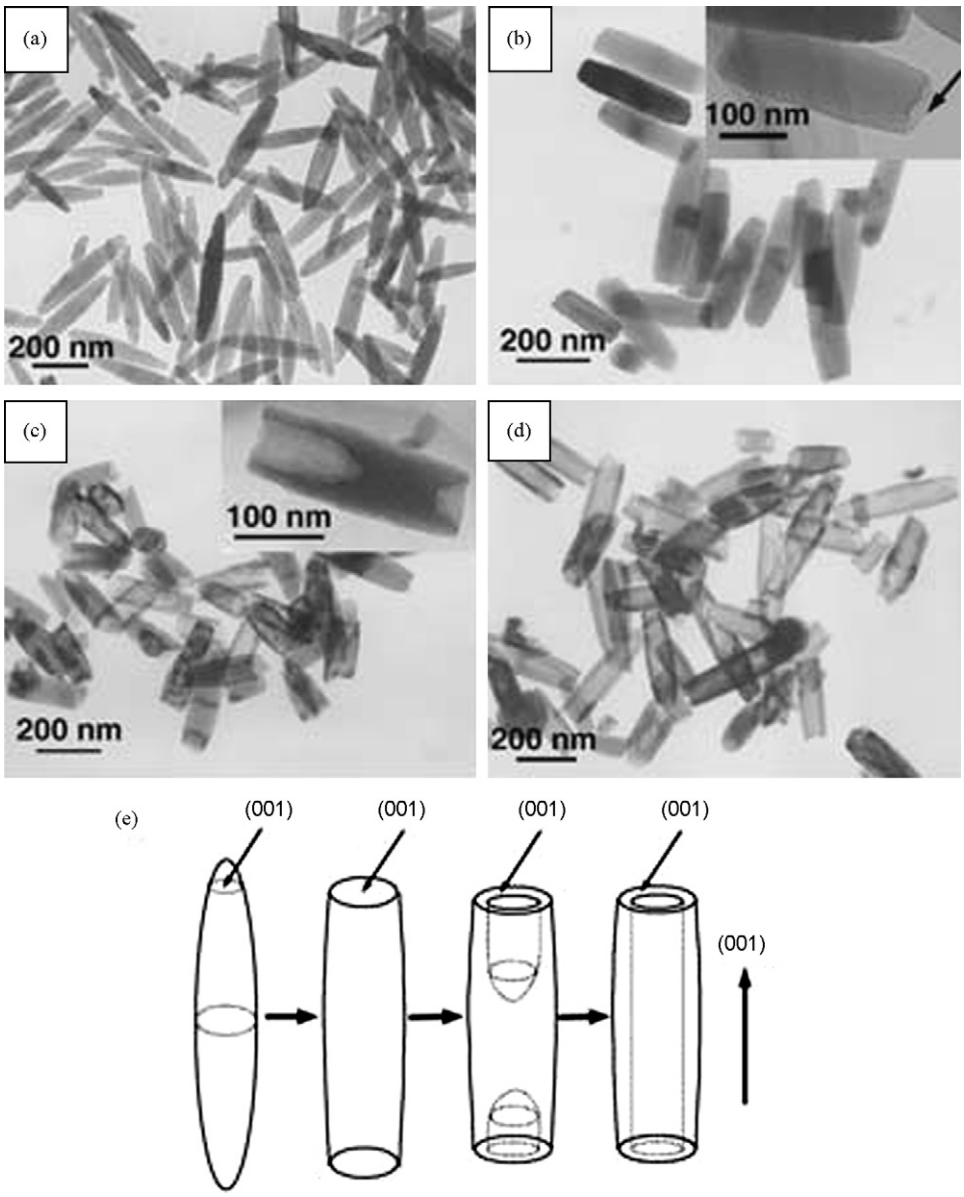

Fig. 13. Morphology evolution of the hematite nanotubes prepared by a phosphate-assisted hydrothermal method with different reaction times. TEM images of the products obtained at 220 °C after 2 h (a), 8 h (b), 12 h (c), and 48 h (d); schematic illustration of the formation process of tubular products (e).
Reprinted with permission from Ref. [133]. Copyright 2009 Wiley-VCH Verlag GmbH & Co. KGaA.

is a special case because the monoclinic phase is more stable under conventional conditions and there is only one V–O–RE bond angle over 90° around each La^{3+} in the monoclinic structures. So $LaVO_4$ is realized as a non-efficient matrix for luminescence materials. We use EDTA to coordinate with La^{3+} to ensure a low metal ion concentration and to slow down the growth process. Meanwhile, we discover that when we use more EDTA, tetragonal $LaVO_4$ can be obtained by a hydrothermal reaction. The detailed mechanism can be explained as a recrystallization process from monoclinic phase to tetragonal phase, which indicates that tetragonal $LaVO_4$ has lower energy than that of monoclinic crystals in the presence of large amount of EDTA molecules. This energy difference is ascribed to the different coordination numbers in two lattice structures. Lanthanum has a coordination number of eight in tetragonal phase $LaVO_4$ and nine in monoclinic phase. With large amount of EDTA in the solution, most of La^{3+} ions are coordinated by EDTA anions. Tetragonal crystals with low coordination number can be obtained in the solution. By doping Eu^{3+} ions, tetragonal $LaVO_4$:Eu nanocrystals are synthesized under similar conditions and exhibit enhanced luminescence intensities compared to the monoclinic $LaVO_4$:Eu (Fig. 11). This new kind of material exhibits high luminescence intensity comparable to commercial tetragonal YVO_4:Eu bulks, but at lower expense. The principles and methods used here are also employed to synthesize other rare earth doped tetragonal $LaVO_4$ nanocrystals with tunable properties reported elsewhere [147,148].

Coordination chemistry is also used for the shape control during the synthesis of $REBO_3$ nanocrystals. Rare earth orthoborates, usually used as vacuum ultraviolet phosphors, benefit from their high vacuum ultraviolet absorption and exceptional optical damage threshold. The traditional solid-phase methods for the synthesis of $REBO_3$ materials usually require high temperatures and long calcination periods. We utilize a mild hydrothermal reaction to synthesize $REBO_3$ nanocrystals. Using rare earth ions and H_3BO_3

as precursors, the formation of $REBO_3$ will release H^+ ions, which increase the solubility of $REBO_3$. Therefore, an alkaline solution should be added in the solution to neutralize these H^+ ions. With urea as the base, $REBO_3$ nanocrystals can be obtained as shown in Fig. 12a [149]. The shape and size of nanocrystals are not regular, because the alkaline condition of the solution will precipitate rare earth ions as $RE(OH)_3$ in a rapid process. $REBO_3$ nanocrystals are formed by a recrystallization process between H_3BO_3 and $RE(OH)_3$. When we use NaOH instead of urea in the hydrothermal reaction, donut-like structured $REBO_3$ nanocrystals are obtained (Fig. 12b) [150]. If we want to obtain $REBO_3$ nanocrystals directly, we have to use some ligands to protect the rare earth ions against OH^-. When we use EDTA as ligand as in the case for rare earth vanadates, we cannot obtain $REBO_3$ nanocrystals at a convenient temperature, because the strong coordination effect between EDTA and rare earth ions will render the concentration of free rare earth ions too low for the growth of nanocrystals. Acetate ions can be used as an alternative ligand to coordinate with rare earth ions [132]. Benefitting from the relatively weak coordination interaction with rare earth ions, acetate ions allow the concentration of rare earth ions to be kept at a higher level than that in the EDTA solutions, which ensure the crystallization of $REBO_3$. The acetic acid/acetate buffer system also consumes the H^+ released during the reaction to improve the yields of the products. Meanwhile, acetate ions also influence the surface energy of different facets of $REBO_3$ nanocrystals. As a result, the YBO_3 nanocrystals as-prepared have drum-like structures, and this effect will be concealed when the reaction temperature is high (Fig. 12c and d). These structures lead to different luminescent properties with Eu^{3+} ion dopants, because the luminescence of Eu^{3+} is very sensitive to the local coordination symmetry [151,152].

For the further understanding of the effect caused by ligands in shape control, Fe_2O_3 nanocrystals can be taken as a typical example other than those rare earth-based nanomaterials. Phosphate anions prove to have strong interactions with Fe_2O_3 crystals because of their high stability constant with Fe^{3+} ions, which results in a large amount of phosphate anions adsorbed on the surface of Fe_2O_3 to reduce the surface energy [153]. In addition, the adsorption of phosphate anions has obvious facet selectivity, so the {0 0 1} facet with least adsorbed phosphate anions will have the highest surface energy. These energy changes cause the Fe_2O_3 crystals to evolve into a spindle shape, growing along the ⟨0 0 1⟩ direction to minimize the area of the {0 0 1} facet. Using this effect, we developed a hydrothermal method to synthesize Fe_2O_3 nanotubes. After the full growth of Fe_2O_3 nanospindles, the concentration of monomer in the solution is not high enough for further growth. Because of the existence of PO_4^{3-}, {0 0 1} facet has the highest surface energy. So the shape evolution of the Fe_2O_3 nanostructures is induced by the dissolution of {0 0 1} facets and further growth of {1 0 0} or some other facets to minimize the surface energy, which can be described as an Ostwald ripening recrystallization process as shown in Fig. 13 [133]. Finally, the inner and outer surface of the nanotubes are composed of {1 0 0} and {1 1 0} facets with lower surface energies. If the dissolution process occurs on the multiple sites on the tip, a novel tube-in-tube structure can be obtained [154]. In order to adjust the aspect ratio of nanotubes, we induced another anion SO_4^{2-} to partly reduce the facet selectivities caused by PO_4^{3-}. SO_4^{2-} can also coordinate to Fe^{3+} ions, but have relatively weak interactions. With a large supply of SO_4^{2-} anions, the surface energy will be leveled between {0 0 1} and other facets. As a result, a series of Fe_2O_3 nanotubes with different aspect ratios can be obtained by the addition of SO_4^{2-} anions, and finally form a ring structure [155]. The Fe_2O_3 nanostructures as-prepared can be reduced at high temperature in a H_2 atmosphere to form Fe_3O_4 nanostructures with their shape preserved. The magnetic properties and the crystallography orientations of these two kinds of nanostructures were also investigated. Using a similar method, tubular rare earth hydroxide nanocrystals were also synthesized by the hydrothermal method by Li et al. [156].

5. Conclusion and outlook

In conclusion, coordination plays a most important role during the synthesis and assembly of nanocrystals. The principles can be summarized as follows.

With an appropriate anion source containing coordinated ligands, single-source precursors can be used in the synthesis of binary compound nanocrystals, which makes it easier to control the crystal growth process, and uses the sources more efficiently.

Coordination creates a metal buffer system during the synthetic process, and this slowly releases metal ions for growth and maintains the concentration of monomer below the nucleation concentration to avoid secondary nucleation, and above the saturation concentration to ensure the growth of nanocrystals. The control can keep the concentration in the size-focus growth stage to obtain monodisperse nanocrystals. Surface-coordinated ligands also affect the surface chemistry of nanocrystals. By virtue of hydrophobic interactions between long carbon chains, the mode of assembly can be tuned by adjusting the polarity of the solvents.

The coordination effect can also influence the shape of nanomaterials during the synthesis process. After the formation of micelles with specific shapes, ligands can coordinate with metal ions and determine the shape of nanocrystals as soft templates. Another effect of capping ligands is the alteration of surface energies for different facets, which further determines the evolution of the morphology of the nanocrystals.

Beyond the points concluded above, the surface ligands can also provide active groups to serve as linkers for the fabrication of hybrid structures with multiple functionalities [157–159].

Although coordination chemistry has proved to exert effective influences on the synthesis, assembly, and surface modification of rare earth functional materials, there are still several questions to be answered for the further development of synthetic routes or the design of new composites. For the control of monomer concentration in the synthesis process for monodisperse nanocrystals, the actual monomer concentration is always difficult to measure in-situ during the reaction. Owing to the lack of effective techniques, the results deduced in Section 3.1 still remain as assumptions, and the actual control operation is more or less empirical. For the shape control of rare earth nanomaterials, the change of surface energy is also an assumption. The calculation parameters for rare earth ions are usually rather complicated, from which the deduction for conclusions are yet still ambiguous. These facts also add to the difficulties in theoretical prediction for these systems, and further investigation is necessary in the future.

Furthermore, the properties of these rare earth base nanomaterials with different size and shape should be investigated. Although the quantum confinement effect is not considered for these materials, the surface effect can be summarized to direct the adjustment of reaction conditions and post treatment method. In addition, polarized luminescence and coupled magnetic properties may be expected in the ordered assemblies composed of shaped nanocrystals with fixed crystal orientation. This could provide a possible motivation for these quasi-crystal assemblies, and promote the requirement for shape and size control in the synthetic process.

Finally, coordination chemistry is a fundamental discipline in inorganic chemistry and nanoscience. The understanding and application of coordination chemistry principle in the new research will reveal some general ideals, which would direct us to find new and better strategies for the synthesis, assembly, and functionalization of nanomaterials. The new discoveries may arise through a combination of ligands and inorganic nanomaterials.

Acknowledgements

The authors would like to thank the NSFC (Nos. 20821091, 20971005, and 20731160001) and MOST of China (No. 2006CB601104) for financial support.

References

[1] A. Trovarelli, Catal. Rev. Sci. Eng. 38 (1996) 439.
[2] J.C.G. Bunzli, Acc. Chem. Res. 39 (2006) 53.
[3] J.C.G. Bunzli, C. Piguet, Chem. Soc. Rev. 34 (2005) 1048.
[4] E.G. Moore, A.P.S. Samuel, K.N. Raymond, Acc. Chem. Res. 42 (2009) 542.
[5] J.M.D. Coey, M. Viret, S. von Molnar, Adv. Phys. 48 (1999) 167.
[6] N. Sabbatini, M. Guardigli, J.M. Lehn, Coord. Chem. Rev. 123 (1993) 201.
[7] R. Sessoli, A.K. Powell, Coord. Chem. Rev. 253 (2009) 2328.
[8] J.R. Heath, Acc. Chem. Res. 32 (1999) 388.
[9] A.M. Morales, C.M. Lieber, Science 279 (1998) 208.
[10] S. Iijima, Nature 354 (1991) 56.
[11] C.B. Murray, D.J. Norris, M.G. Bawendi, J. Am. Chem. Soc. 115 (1993) 8706.
[12] M. Brust, M. Walker, D. Bethell, D.J. Schiffrin, R. Whyman, Chem. Commun. (1994) 801.
[13] S.H. Sun, C.B. Murray, D. Weller, L. Folks, A. Moser, Science 287 (2000) 1989.
[14] Y.N. Xia, P.D. Yang, Y.G. Sun, Y.Y. Wu, B. Mayers, B. Gates, Y.D. Yin, F. Kim, Y.Q. Yan, Adv. Mater. 15 (2003) 353.
[15] Y. Wang, N. Herron, J. Phys. Chem. 95 (1991) 525.
[16] T. Takagahara, K. Takeda, Phys. Rev. B 46 (1992) 15578.
[17] B.O. Dabbousi, J. RodriguezViejo, F.V. Mikulec, J.R. Heine, H. Mattoussi, R. Ober, K.F. Jensen, M.G. Bawendi, J. Phys. Chem. B 101 (1997) 9463.
[18] J. Shen, L.D. Sun, C.H. Yan, Dalton Trans. (2008) 5687.
[19] F. Wang, X.G. Liu, Chem. Soc. Rev. 38 (2009) 976.
[20] Z.G. Yan, C.H. Yan, J. Mater. Chem. 18 (2008) 5046.
[21] F. Vetrone, J.A. Capobianco, Int. J. Nanotechnol. 5 (2008) 1306.
[22] A. Ghezelbash, M.B. Sigman, B.A. Korgel, Nano Lett. 4 (2004) 537.
[23] M.A. Malik, N. Revaprasadu, P. O'Brien, Chem. Mater. 13 (2001) 913.
[24] M.B. Sigman, A. Ghezelbash, T. Hanrath, A.E. Saunders, F. Lee, B.A. Korgel, J. Am. Chem. Soc. 125 (2003) 16050.
[25] Y.W. Zhang, X. Sun, R. Si, L.P. You, C.H. Yan, J. Am. Chem. Soc. 127 (2005) 3260.
[26] Y.P. Du, Y.W. Zhang, L.D. Sun, C.H. Yan, Dalton Trans. (2009) 8574.
[27] R. Si, Y.W. Zhang, L.P. You, C.H. Yan, Angew. Chem. Int. Ed. 44 (2005) 3256.
[28] R. Si, Y.W. Zhang, H.P. Zhou, L.D. Sun, C.H. Yan, Chem. Mater. 19 (2007) 18.
[29] F. Zhao, H.L. Sun, G. Su, S. Gao, Small 2 (2006) 244.
[30] F. Zhao, M. Yuan, W. Zhang, S. Gao, J. Am. Chem. Soc. 128 (2006) 11758.
[31] F. Zhao, S. Gao, J. Mater. Chem. 18 (2008) 949.
[32] M.A. El-Sayed, Acc. Chem. Res. 34 (2001) 257.
[33] M.C. Daniel, D. Astruc, Chem. Rev. 104 (2004) 293.
[34] A.P. Alivisatos, Science 271 (1996) 933.
[35] Y.G. Sun, Y.N. Xia, Science 298 (2002) 2176.
[36] K.L. Kelly, E. Coronado, L.L. Zhao, G.C. Schatz, J. Phys. Chem. B 107 (2003) 668.
[37] Y.W. Jun, J.S. Choi, J. Cheon, Angew. Chem. Int. Ed. 45 (2006) 3414.
[38] M.P. Pileni, J. Phys. Chem. C 111 (2007) 9019.
[39] J.H. Fendler, F.C. Meldrum, Adv. Mater. 7 (1995) 607.
[40] M.P. Pileni, Nat. Mater. 2 (2003) 145.
[41] B.L. Cushing, V.L. Kolesnichenko, C.J. O'Connor, Chem. Rev. 104 (2004) 3893.
[42] J.W. Mullin, Crystallization, 4th ed., Butterworth-Heinemann, Oxford, Boston, 2001.
[43] H.E. Buckley, Crystal Growth, Chapman and Hall, London, 1952.
[44] M. Davies, P. Johnson, A.F. Wells, H.M. Powell, Annu. Rep. Prog. Chem. 43 (1946) 5.
[45] V.K. Lamer, R.H. Dinegar, J. Am. Chem. Soc. 72 (1950) 4847.
[46] T. Sugimoto, Adv. Colloid Interface Sci. 28 (1987) 65.
[47] X.G. Peng, J. Wickham, A.P. Alivisatos, J. Am. Chem. Soc. 120 (1998) 5343.
[48] A.K. Levine, F.C. Palilla, Appl. Phys. Lett. 5 (1964) 118.
[49] K. Riwotzki, M. Haase, J. Phys. Chem. B 105 (2001) 12709.
[50] H. Meyssamy, K. Riwotzki, A. Kornowski, S. Naused, M. Haase, Adv. Mater. 11 (1999) 840.
[51] K. Riwotzki, H. Meyssamy, H. Schnablegger, A. Kornowski, M. Haase, Angew. Chem. Int. Ed. 40 (2001) 573.
[52] K. Kompe, H. Borchert, J. Storz, A. Lobo, S. Adam, T. Moller, M. Haase, Angew. Chem. Int. Ed. 42 (2003) 5513.
[53] S. Heer, O. Lehmann, M. Haase, H.U. Gudel, Angew. Chem. Int. Ed. 42 (2003) 3179.
[54] K. Riwotzki, M. Haase, J. Phys. Chem. B 102 (1998) 10129.
[55] A. Huignard, T. Gacoin, J.P. Boilot, Chem. Mater. 12 (2000) 1090.
[56] J.Q. Gu, J. Shen, L.D. Sun, C.H. Yan, J. Phys. Chem. C 112 (2008) 6589.
[57] J.Q. Gu, L.D. Sun, Z.G. Yan, C.H. Yan, Chem. Asian J. 3 (2008) 1857.
[58] R. Si, Y.W. Zhang, C.X. Xiao, S.J. Li, B.X. Lin, Y. Kou, C.H. Yan, Phys. Chem. Chem. Phys. 6 (2004) 1056.
[59] Y.W. Zhang, R. Si, C.S. Liao, C.H. Yan, J. Phys. Chem. B 107 (2003) 10159.
[60] R. Si, Y.W. Zhang, L.M. Wang, S.J. Li, B.X. Lin, W.S. Chu, Z.Y. Wu, C.H. Yan, J. Phys. Chem. C 111 (2007) 787.
[61] R. Si, Y.W. Zhang, S.J. Li, B.X. Lin, C.H. Yan, J. Phys. Chem. B 108 (2004) 12481.
[62] V.F. Puntes, K.M. Krishnan, P. Alivisatos, Appl. Phys. Lett. 78 (2001) 2187.
[63] V.F. Puntes, D. Zanchet, C.K. Erdonmez, A.P. Alivisatos, J. Am. Chem. Soc. 124 (2002) 12874.
[64] T. Hyeon, S.S. Lee, J. Park, Y. Chung, H. Bin Na, J. Am. Chem. Soc. 123 (2001) 12798.
[65] S.H. Sun, H. Zeng, D.B. Robinson, S. Raoux, P.M. Rice, S.X. Wang, G.X. Li, J. Am. Chem. Soc. 126 (2004) 273.
[66] X.H. Zhong, Y.Y. Feng, W. Knoll, M.Y. Han, J. Am. Chem. Soc. 125 (2003) 13559.
[67] R. Sivakumar, F.C.J.M. van Veggel, M. Raudsepp, J. Am. Chem. Soc. 127 (2005) 12464.
[68] J.W. Stouwdam, F.C.J.M. van Veggel, Nano Lett. 2 (2002) 733.
[69] G.A. Hebbink, J.W. Stouwdam, D.N. Reinhoudt, F.C.J.M. van Veggel, Adv. Mater. 14 (2002) 1147.
[70] X. Sun, Y.W. Zhang, Y.P. Du, Z.G. Yan, R. Si, L.P. You, C.H. Yan, Chem. Eur. J. 13 (2007) 2320.
[71] H.X. Mai, Y.W. Zhang, R. Si, Z.G. Yan, L.D. Sun, L.P. You, C.H. Yan, J. Am. Chem. Soc. 128 (2006) 6426.
[72] H.X. Mai, Y.W. Zhang, L.D. Sun, C.R. Yan, J. Phys. Chem. C 111 (2007) 13730.
[73] H.X. Mai, Y.W. Zhang, L.D. Sun, C.H. Yan, J. Phys. Chem. C 111 (2007) 13721.
[74] J.C. Boyer, L.A. Cuccia, J.A. Capobianco, Nano Lett. 7 (2007) 847.
[75] J.C. Boyer, F. Vetrone, L.A. Cuccia, J.A. Capobianco, J. Am. Chem. Soc. 128 (2006) 7444.
[76] G.S. Yi, G.M. Chow, Adv. Funct. Mater. 16 (2006) 2324.
[77] D.K. Chatteriee, A.J. Rufalhah, Y. Zhang, Biomaterials 29 (2008) 937.
[78] Z.Q. Li, Y. Zhang, S. Jiang, Adv. Mater. 20 (2008) 4765.
[79] W. Feng, L.D. Sun, Y.W. Zhang, C.H. Yan, Small 5 (2009) 2057.
[80] Y.P. Du, Y.W. Zhang, Z.G. Yan, L.D. Sun, S. Gao, C.H. Yan, Chem. Asian J. 2 (2007) 965.
[81] H.P. Zhou, Y.W. Zhang, R. Si, L.S. Zhang, W.G. Song, C.H. Yan, J. Phys. Chem. C 112 (2008) 20366.
[82] H.X. Mai, Y.W. Zhang, L.D. Sun, C.H. Yan, Chem. Mater. 19 (2007) 4514.
[83] C.B. Murray, C.R. Kagan, M.G. Bawendi, Science 270 (1995) 1335.
[84] Y. Yin, A.P. Alivisatos, Nature 437 (2005) 664.
[85] C.P. Collier, T. Vossmeyer, J.R. Heath, Annu. Rev. Phys. Chem. 49 (1998) 371.
[86] A. Courty, A. Mermet, P.A. Albouy, E. Duval, M.P. Pileni, Nat. Mater. 4 (2005) 395.
[87] C.B. Murray, C.R. Kagan, M.G. Bawendi, Annu. Rev. Mater. Sci. 30 (2000) 545.
[88] A.R. Tao, D.P. Ceperley, P. Sinsermsuksakul, A.R. Neureuther, P.D. Yang, Nano Lett. 8 (2008) 4033.
[89] E.V. Shevchenko, M. Ringler, A. Schwemer, D.V. Talapin, T.A. Klar, A.L. Rogach, J. Feldmann, A.P. Alivisatos, J. Am. Chem. Soc. 130 (2008) 3274.
[90] J.P. Ge, Y.X. Hu, Y.D. Yin, Angew. Chem. Int. Ed. 46 (2007) 7428.
[91] M.H. Huang, S. Mao, H. Feick, H.Q. Yan, Y.Y. Wu, H. Kind, E. Weber, R. Russo, P.D. Yang, Science 292 (2001) 1897.
[92] C.A. Mirkin, R.L. Letsinger, R.C. Mucic, J.J. Storhoff, Nature 382 (1996) 607.
[93] F. Bai, D.S. Wang, Z.Y. Huo, W. Chen, L.P. Liu, X. Liang, C. Chen, X. Wang, Q. Peng, Y.D. Li, Angew. Chem. Int. Ed. 46 (2007) 6650.
[94] P.V. Braun, P. Osenar, S.I. Stupp, Nature 380 (1996) 325.
[95] A.M. Kalsin, M. Fialkowski, M. Paszewski, S.K. Smoukov, K.J.M. Bishop, B.A. Grzybowski, Science 312 (2006) 420.
[96] W. Shenton, D. Pum, U.B. Sleytr, S. Mann, Nature 389 (1997) 585.
[97] E.V. Shevchenko, D.V. Talapin, N.A. Kotov, S. O'Brien, C.B. Murray, Nature 439 (2006) 55.
[98] E.V. Shevchenko, D.V. Talapin, C.B. Murray, S. O'Brien, J. Am. Chem. Soc. 128 (2006) 3620.
[99] N.D. Denkov, O.D. Velev, P.A. Kralchevsky, I.B. Ivanov, H. Yoshimura, K. Nagayama, Langmuir 8 (1992) 3183.
[100] P.A. Kralchevsky, K. Nagayama, Langmuir 10 (1994) 23.
[101] K.J.M. Bishop, C.E. Wilmer, S. Soh, B.A. Grzybowski, Small 5 (2009) 1600.
[102] S.A. Harfenist, Z.L. Wang, R.L. Whetten, I. Vezmar, M.M. Alvarez, Adv. Mater. 9 (1997) 817.
[103] Y.P. Du, Y.W. Zhang, L.D. Sun, C.H. Yan, J. Am. Chem. Soc. 131 (2009) 3162.
[104] C.J. Murphy, N.R. Jana, Adv. Mater. 14 (2002) 80.
[105] G.A. Ozin, Adv. Mater. 4 (1992) 612.
[106] T.S. Ahmadi, Z.L. Wang, T.C. Green, A. Henglein, M.A. ElSayed, Science 272 (1996) 1924.
[107] C.Z. Wu, Y. Xie, Chem. Commun. (2009) 5943.
[108] J.C. Hulteen, C.R. Martin, J. Mater. Chem. 7 (1997) 1075.
[109] B.B. Lakshmi, P.K. Dorhout, C.R. Martin, Chem. Mater. 9 (1997) 857.
[110] D. Almawlawi, C.Z. Liu, M. Moskovits, J. Mater. Res. 9 (1994) 1014.
[111] M.P. Pileni, J. Phys. Chem. 97 (1993) 6961.
[112] Y.P. Du, X. Sun, Y.W. Zhang, Z.G. Yan, L.D. Sun, C.H. Yan, Cryst. Growth Des. 9 (2009) 2013.
[113] Z.Q. Li, J. Tao, X.M. Lu, Y.M. Zhu, Y.N. Xia, Nano Lett. 8 (2008) 3052.
[114] Z.Y. Huo, C.K. Tsung, W.Y. Huang, X.F. Zhang, P.D. Yang, Nano Lett. 8 (2008) 2041.
[115] J.S. Son, X.D. Wen, J. Joo, J. Chae, S.I. Baek, K. Park, J.H. Kim, K. An, J.H. Yu, S.G. Kwon, S.H. Choi, Z.W. Wang, Y.W. Kim, Y. Kuk, R. Hoffmann, T. Hyeon, Angew. Chem. Int. Ed. 48 (2009) 6861.
[116] C.T. Kresge, M.E. Leonowicz, W.J. Roth, J.C. Vartuli, J.S. Beck, Nature 359 (1992) 710.
[117] A. Corma, Chem. Rev. 97 (1997) 2373.
[118] P.T. Tanev, T.J. Pinnavaia, Science 267 (1995) 865.
[119] Q. Yuan, Q. Liu, W.G. Song, W. Feng, W.L. Pu, L.D. Sun, Y.W. Zhang, C.H. Yan, J. Am. Chem. Soc. 129 (2007) 6698.
[120] Q. Yuan, Y. Liu, L.L. Li, Z.X. Li, C.J. Fang, W.T. Duan, X.G. Li, C.H. Yan, Microporous Mesoporous Mater. 124 (2009) 169.
[121] Q. Yuan, L.L. Li, S.L. Lu, H.H. Duan, Z.X. Li, Y.X. Zhu, C.H. Yan, J. Phys. Chem. C 113 (2009) 4117.

[122] Q. Yuan, A.X. Yin, C. Luo, L.D. Sun, Y.W. Zhang, W.T. Duan, H.C. Liu, C.H. Yan, J. Am. Chem. Soc. 130 (2008) 3465.
[123] Z.L. Wang, J. Phys. Chem. B 104 (2000) 1153.
[124] X.G. Peng, L. Manna, W.D. Yang, J. Wickham, E. Scher, A. Kadavanich, A.P. Alivisatos, Nature 404 (2000) 59.
[125] Z.A. Peng, X.G. Peng, J. Am. Chem. Soc. 123 (2001) 1389.
[126] A. Puzder, A.J. Williamson, N. Zaitseva, G. Galli, L. Manna, A.P. Alivisatos, Nano Lett. 4 (2004) 2361.
[127] W.J. Zhang, Y. Liu, R.G. Cao, Z.H. Li, Y.H. Zhang, Y. Tang, K.N. Fan, J. Am. Chem. Soc. 130 (2008) 15581.
[128] Y.G. Sun, Y.D. Yin, B.T. Mayers, T. Herricks, Y.N. Xia, Chem. Mater. 14 (2002) 4736.
[129] I. Washio, Y.J. Xiong, Y.D. Yin, Y.N. Xia, Adv. Mater. 18 (2006) 1745.
[130] A. Tao, P. Sinsermsuksakul, P.D. Yang, Angew. Chem. Int. Ed. 45 (2006) 4597.
[131] F. Luo, C.J. Jia, W. Song, L.P. You, C.H. Yan, Cryst. Growth Des. 5 (2005) 137.
[132] X.C. Jiang, L.D. Sun, W. Feng, C.H. Yan, Cryst. Growth Des. 4 (2004) 517.
[133] C.J. Jia, L.D. Sun, Z.G. Yan, L.P. You, F. Luo, X.D. Han, Y.C. Pang, Z. Zhang, C.H. Yan, Angew. Chem. Int. Ed. 44 (2005) 4328.
[134] T.X.T. Sayle, S.C. Parker, C.R.A. Catlow, Surf. Sci. 316 (1994) 329.
[135] Z.L. Wang, X.D. Feng, J. Phys. Chem. B 107 (2003) 13563.
[136] T.X.T. Sayle, S.C. Parker, D.C. Sayle, Chem. Commun. (2004) 2438.
[137] D.C. Sayle, S.A. Maicaneanu, G.W. Watson, J. Am. Chem. Soc. 124 (2002) 11429.
[138] E. Aneggi, J. Llorca, M. Boaro, A. Trovarelli, J. Catal. 234 (2005) 88.
[139] K.B. Zhou, X. Wang, X.M. Sun, Q. Peng, Y.D. Li, J. Catal. 229 (2005) 206.
[140] H.X. Mai, L.D. Sun, Y.W. Zhang, R. Si, W. Feng, H.P. Zhang, H.C. Liu, C.H. Yan, J. Phys. Chem. B 109 (2005) 24380.
[141] N.V. Skorodumova, M. Baudin, K. Hermansson, Phys. Rev. B 69 (2004).
[142] S.W. Yang, L. Gao, J. Am. Chem. Soc. 128 (2006) 9330.
[143] J. Zhang, S. Ohara, M. Umetsu, T. Naka, Y. Hatakeyama, T. Adschiri, Adv. Mater. 19 (2007) 203.
[144] K. Kaneko, K. Inoke, B. Freitag, A.B. Hungria, P.A. Midgley, T.W. Hansen, J. Zhang, S. Ohara, T. Adschiri, Nano Lett. 7 (2007) 421.
[145] W. Feng, L.D. Sun, C.H. Yan, unpublished results.
[146] C.J. Jia, L.D. Sun, F. Luo, X.C. Jiang, L.H. Wei, C.H. Yan, Appl. Phys. Lett. 84 (2004) 5305.
[147] W.L. Fan, Y.X. Bu, X.Y. Song, S.X. Sun, X.A. Zhao, Cryst. Growth Des. 7 (2007) 2361.
[148] W.L. Fan, X.Y. Song, Y.X. Bu, S.X. Sun, X. Zhao, J. Phys. Chem. B 110 (2006) 23247.
[149] X.C. Jiang, C.H. Yan, L.D. Sun, Z.G. Wei, C.S. Liao, J. Solid State Chem. 175 (2003) 245.
[150] X.C. Jiang, L.D. Sun, C.H. Yan, J. Phys. Chem. B 108 (2004) 3387.
[151] C.H. Yan, L.D. Sun, C.S. Liao, Y.X. Zhang, Y.Q. Lu, S.H. Huang, S.Z. Lu, Appl. Phys. Lett. 82 (2003) 3511.
[152] Z.G. Wei, L.D. Sun, C.S. Liao, J.L. Yin, X.C. Jiang, C.H. Yan, S.Z. Lu, J. Phys. Chem. B 106 (2002) 10610.
[153] J.D. Russell, R.L. Parfitt, A.R. Fraser, V.C. Farmer, Nature 248 (1974) 220.
[154] C.J. Jia, L.D. Sun, Z.G. Yan, Y.C. Pang, L.P. You, C.H. Yan, J. Phys. Chem. C 111 (2007) 13022.
[155] C.J. Jia, L.D. Sun, F. Luo, X.D. Han, L.J. Heyderman, Z.G. Yan, C.H. Yan, K. Zheng, Z. Zhang, M. Takano, N. Hayashi, M. Eltschka, M. Klaui, U. Rudiger, T. Kasama, L. Cervera-Gontard, R.E. Dunin-Borkowski, G. Tzvetkov, J. Raabe, J. Am. Chem. Soc. 130 (2008) 16968.
[156] W.J. Li, X. Wang, Y.D. Li, Chem. Commun. (2004) 164.
[157] I.L. Medintz, H.T. Uyeda, E.R. Goldman, H. Mattoussi, Nat. Mater. 4 (2005) 435.
[158] Z.G. Chen, H.L. Chen, H. Hu, M.X. Yu, F.Y. Li, Q. Zhang, Z.G. Zhou, T. Yi, C.H. Huang, J. Am. Chem. Soc. 130 (2008) 3023.
[159] H.P. Zhou, C.H. Xu, W. Sun, C.H. Yan, 19 (2009) 3892.